



HAL
open science

Global carbon budgets simulated by the Beijing Climate Center Climate System Model for the last century

T. Wu, W. Li, J. Ji, X. Xin, Laurent Li, Z. Wang, Y. Zhang, J. Li, F. Zhang, M. Wei, et al.

► To cite this version:

T. Wu, W. Li, J. Ji, X. Xin, Laurent Li, et al.. Global carbon budgets simulated by the Beijing Climate Center Climate System Model for the last century. *Journal of Geophysical Research: Atmospheres*, 2013, 118 (10), pp.4326-4347. 10.1002/jgrd.50320 . hal-01092294

HAL Id: hal-01092294

<https://hal.science/hal-01092294>

Submitted on 22 Oct 2021

HAL is a multi-disciplinary open access archive for the deposit and dissemination of scientific research documents, whether they are published or not. The documents may come from teaching and research institutions in France or abroad, or from public or private research centers.

L'archive ouverte pluridisciplinaire **HAL**, est destinée au dépôt et à la diffusion de documents scientifiques de niveau recherche, publiés ou non, émanant des établissements d'enseignement et de recherche français ou étrangers, des laboratoires publics ou privés.



Distributed under a Creative Commons Attribution - NonCommercial - ShareAlike 4.0 International License

Global carbon budgets simulated by the Beijing Climate Center Climate System Model for the last century

Tongwen Wu,^{1,2} Weiping Li,^{1,2} Jinjun Ji,^{1,3} Xiaoge Xin,^{1,2} Laurent Li,^{1,4} Zaizhi Wang,^{1,2} Yanwu Zhang,^{1,2} Jianglong Li,^{1,2} Fang Zhang,^{1,2} Min Wei,⁵ Xueli Shi,^{1,2} Fanghua Wu,^{1,2} Li Zhang,^{1,2} Min Chu,^{1,2} Weihua Jie,^{1,2} Yiming Liu,^{1,2} Fang Wang,^{1,2} Xiangwen Liu,^{1,2} Qiaoping Li,^{1,2} Min Dong,^{1,2} Xiaoyun Liang,^{1,2} Yang Gao,^{1,2} and Jie Zhang^{1,2}

Received 29 February 2012; revised 23 January 2013; accepted 3 March 2013; published 29 May 2013.

[1] The paper examines terrestrial and oceanic carbon budgets from preindustrial time to present day in the version of Beijing Climate Center Climate System Model (BCC_CSM1.1) which is a global fully coupled climate-carbon cycle model. Atmospheric CO₂ concentration is calculated from a prognostic equation taking into account global anthropogenic CO₂ emissions and the interactive CO₂ exchanges of land-atmosphere and ocean-atmosphere. When forced by prescribed historical emissions of CO₂ from combustion of fossil fuels and land use change, BCC_CSM1.1 can reproduce the trends of observed atmospheric CO₂ concentration and global surface air temperature from 1850 to 2005. Simulated interannual variability and long-term trend of global carbon sources and sinks and their spatial patterns generally agree with other model estimates and observations, which shows the following: (1) Both land and ocean in the last century act as net carbon sinks. The ability of carbon uptake by land and ocean is enhanced at the end of last century. (2) Interannual variability of the global atmospheric CO₂ concentration is closely correlated with the El Niño-Southern Oscillation cycle, in agreement with observations. (3) Interannual variation of the land-to-atmosphere net carbon flux is positively correlated with surface air temperature while negatively correlated with soil moisture over low and midlatitudes. The relative contribution of soil moisture to the interannual variation of land-atmosphere CO₂ exchange is more important than that of air temperature over tropical regions, while surface air temperature is more important than soil moisture over other regions of the globe.

Citation: Wu, T., et al. (2013), Global carbon budgets simulated by the Beijing Climate Center Climate System Model for the last century, *J. Geophys. Res. Atmos.*, 118, 4326–4347, doi:10.1002/jgrd.50320.

1. Introduction

[2] It has been well documented that human activities are enhancing the greenhouse effect of the atmosphere and altering the global climate [Le Treut et al., 2007]. The increase

of global temperature during the last 150 years can be at least partially attributed to the increase of atmospheric CO₂ concentration as a consequence of anthropogenic activities including combustion of fossil fuels, cement production, and land use-associated emission [Houghton et al., 2001]. At global scale, however, only about half of the anthropogenic carbon emissions have been stored in the atmosphere, while the remainder has been absorbed by oceans and terrestrial biosphere [Prentice et al., 2001].

[3] Increase of CO₂ in the atmosphere and the consequent climate change may modify behaviors of the terrestrial ecosystems and ocean biogeochemistry, which is susceptible to introduce important feedbacks in the earth system. Increasing attention has been paid to this issue in the scientific literature [e.g., Sarmiento and Le Quéré, 1996; Sarmiento et al., 1998; Cox et al., 2000; Cramer et al., 2001; Dufresne et al., 2002; Wigley, 2005; Friedlingstein et al., 2001, 2003, 2006; Matthews et al., 2005; Meehl and Coauthors, 2007; Arora et al., 2009; Gregory et al., 2009; Randerson et al., 2009; Boer and Arora, 2010; Cadule et al., 2010; Roy et al.,

¹Beijing Climate Center, China Meteorological Administration, Beijing, China.

²Laboratory for Climate Studies, China Meteorological Administration, Beijing, China.

³Institute of Atmospheric Physics, Chinese Academy of Sciences, Beijing, China.

⁴Laboratoire de Météorologie Dynamique, IPSL, CNRS/UPMC, Paris, France.

⁵National Meteorological Information Center, China Meteorological Administration, Beijing, China.

Corresponding author: T. Wu, National Climate Center, China Meteorological Administration, 46 Zhongguancun Nandajie, Beijing 100081, China. (twuwu@cma.gov.cn)

2011; Vichi *et al.*, 2011; Zickfeld *et al.*, 2011]. Friedlingstein and Prentice [2010] gave a review of earlier works on carbon-climate feedback and concluded that global warming leads to an additional release of CO₂ from the land/ocean system to the atmosphere on timescales ranging from interannual to millennial. Zickfeld *et al.* [2011] reported that strong nonlinearity exists in carbon-climate feedbacks.

[4] Studies in the past several years also revealed existence of large uncertainties in estimation of terrestrial and oceanic carbon uptake. Bolin and Sukumar [2000] showed that terrestrial carbon uptake was in the range of 0.6 to 3.2 GtC yr⁻¹ (gigatons of carbon per year) for the 1980s and 1.0 to 3.6 GtC yr⁻¹ for the 1990s. These numbers have been revised by House *et al.* [2003], who reported that terrestrial carbon uptake was in the range of 0.3 to 4.0 GtC yr⁻¹ and 1.6 to 4.8 GtC yr⁻¹ for the 1980s and 1990s, respectively. Le Quéré [2010] presented a new estimate of the present-day global carbon budget and pointed out that about 45% of the total CO₂ emitted from fossil fuel burning and land use change stayed in the atmosphere on average during the past decades. They also suggested that the efficiency of carbon sinks could have already decreased in the past decades. Considerable uncertainty exists not only in magnitude but also in locations of the carbon sinks and sources [Friedlingstein *et al.*, 2006; Boer and Arora, 2010]. Cadule *et al.* [2010] pointed out that uncertainty in the amplitude of climate-carbon feedback is mainly due to uncertainty of the response of the terrestrial biosphere to climate change. Various processes contribute to the uncertainty, including temperature dependence of heterotrophic respiration [Cox *et al.*, 2000; Prentice *et al.*, 2001; Zeng *et al.*, 2004], amount of primary productivity [Matthews *et al.*, 2005], vertical mixing in oceans [Friedlingstein *et al.*, 2003], and cycling of carbon in the living biomass especially in the tropical forest [Cox *et al.*, 2004; Denman *et al.*, 2007].

[5] One obstacle in investigation of the carbon cycle is the difficulty in obtaining direct observational estimates of carbon uptake. Climate models are, at present, the most advanced tool to investigate carbon budget and to project future climate. The Coupled Carbon Cycle Climate Model Intercomparison Project (C⁴MIP) was initiated to evaluate uncertainties of climate-carbon feedbacks [Trenberth *et al.*, 2007]. A few works have already been reported from the scientific community [e.g., Randerson *et al.*, 2009; Cadule *et al.*, 2010; Roy *et al.*, 2011]. Recent studies are coordinated in the phase five of the Coupled Model Intercomparison Project (CMIP5). One main motivation of CMIP5 is to address relevant scientific questions on carbon-climate interactions [Taylor *et al.*, 2009]. The Beijing Climate Center Climate System Model version BCC_CSM1.1 is one of the comprehensive carbon-climate models joining the CMIP5 efforts to support the Intergovernmental Panel on Climate Change (IPCC) AR5.

[6] An accurate simulation of the 20th century global carbon cycle is a prerequisite to reliably project future climate. The purpose of this paper is to evaluate BCC_CSM in reproducing the global carbon cycle from 1850 to 2005 and to quantify the simulated carbon sources and sinks from interannual variability to long-term trend. We also provide some discussions on results of BCC_CSM compared to those of other models.

[7] A relevant description on the model and experiments is firstly presented in section 2. Regional and global characteristics of the simulated land-atmosphere and ocean-atmosphere carbon exchange compared to estimates from other studies are analyzed in section 3.

2. Model Description and Experiments

[8] The model used in this work is the version 1.1 of the Beijing Climate Center Climate System Model (BCC_CSM1.1) developed at the Beijing Climate Center (BCC), China Meteorological Administration (CMA). BCC_CSM1.1 is a fully coupled global climate-carbon model including interactive vegetation and global carbon cycle, in which the atmospheric component BCC Atmospheric General Model version 2.1 (BCC_AGCM2.1), ocean component Modular Ocean Model version 4 (MOM4)-L40, land component BCC Atmosphere and Vegetation Interaction Model version 1.0 (BCC_AVIM1.0), and sea ice component [sea ice simulator (SIS)] are fully coupled and interact with each other through fluxes of momentum, energy, water, and carbon at their interfaces. Information between the atmosphere and the ocean is exchanged once per simulated day. The exchange of atmospheric carbon with the land biosphere is calculated at each model time step (20 min).

2.1. The Atmospheric Model

[9] The atmospheric component in BCC_CSM1.1 is the Beijing Climate Center Atmospheric General Circulation Model version 2.1 (BCC_AGCM2.1). It is a global spectral model with a horizontal resolution of T42, approximately 2.8125° × 2.8125° transformed grid, and 26 levels in a hybrid sigma/pressure vertical coordinate system with the top level at 2.914 hPa. The dynamical core of the model is described in Wu *et al.* [2008] and a precedent version, BCC_AGCM2.0, is detailed in Wu *et al.* [2010]. The governing equations of the model are originated from the Eulerian dynamics in the Community Atmosphere Model (CAM3) [Collins *et al.*, 2004], but substantial changes concerning the governing equations and their resolving technique (use of reference atmospheric temperature and surface pressure) have been implemented in BCC. Most of the physical processes are from CAM3 developed by the National Center for Atmospheric Research (NCAR). A few new schemes are implemented, including parameterizations for the deep cumulus convection, dry adiabatic adjustment, latent heat and sensible heat fluxes over ocean surface, and snow cover fraction [Wu *et al.*, 2010]. BCC-AGCM2.1 is an updated version of BCC_AGCM2.0 with a new deep penetrative convection scheme as described in Wu [2012]. Furthermore, CO₂ is a prognostic variable in BCC-AGCM2.1. It is no more a passive tracer, and it is calculated through a budget equation, as a function of global-integrated anthropogenic CO₂ emissions, and interactive CO₂ fluxes at the interfaces with land and ocean. For the time being, CO₂ is homogeneously distributed for the whole atmosphere since we do not take into account its spatial variability due to atmospheric circulation and chemical processes.

[10] The atmospheric CO₂ concentration (CO_{2atm}) can be formulated as

$$\frac{\partial \text{CO}_2 \text{ atm}(t)}{\partial t} = E_{\text{fossil}} + E_{\text{landuse}} + F_{\text{land}} + F_{\text{ocean}} \quad (1)$$

where t is the time, E_{fossil} and E_{landuse} are the CO_2 emissions due to fossil fuel consumption and cement manufacture, and land use change (including wood harvest), respectively. The CO_2 emission data (the total of E_{fossil} and E_{landuse}) from the years 1850 to 2005 were CMIP5-recommended (available from <http://cmip-pcmdi.llnl.gov/cmip5/>) and created by *Meinshausen et al.* [2011]. F_{land} and F_{ocean} in equation (1) are the carbon exchange rates with land and ocean (positive as a flux to atmosphere), respectively. So, negative F_{land} and F_{ocean} represent the net uptake by the land vegetation-soil system and the ocean, respectively.

2.2. The Land Model

[11] The land model in BCC_CSM1.1 is the Beijing Climate Center Atmosphere and Vegetation Interaction Model version 1.0 (BCC_AVIM1.0). It is a comprehensive land surface model and can be coupled into the BCC_CSM1.1 to simulate land surface biogeophysical and plant ecophysiological processes. There are exchanges of energy, water, and carbon between land surface and the atmosphere.

[12] BCC_AVIM1.0 is originated from the Atmosphere and Vegetation Interaction Model (AVIM) [*Ji, 1995; Lu and Ji, 2006; Ji et al. 2008*] and includes three submodules: biogeophysical, ecophysiological, and soil carbon-nitrogen dynamical modules. A modified biogeophysical framework with 10 layer soil and at most five layer snow is almost the same as that in the NCAR Community Land Model version 3.0 (CLM3) [*Oleson et al., 2004*]. Since the snow cover fraction (SCF) is underestimated in Bermuda Atlantic Time-series Study [*Yang et al., 1997*] and CLM3, we adopted a scheme of SCF from the work of *Yang et al.* [1997] and *Roesch et al.* [2001] which takes into account the influence of subgrid topography variability on SCF.

$$f_{\text{sno}} = \tanh\left(\frac{h_{\text{sno}}}{2.5z_{0g}}\right) \cdot \sqrt{\frac{S_n}{S_n + \varepsilon + 0.01\sigma_z}} \quad (2)$$

where f_{sno} represents SCF, h_{sno} snow depth (m), z_{0g} roughness length of bare soil, S_n snow water equivalence (mm), σ_z the spatial variance of topography (m) in the grid cell, and ε a minute constant (0.0001).

[13] The terrestrial carbon cycle in BCC_AVIM1.0 operates through a series of biochemical and physiological processes on photosynthesis and respiration of vegetation. There is a seasonally varying allocation of carbohydrate to leaves, stem, and root tissues in function of the prognostic leaf area index. Our model also takes into account carbon loss due to turnover and mortality of vegetation, and CO_2 release into atmosphere through soil respiration. The vegetation litter to the ground surface and into the soil is divided into eight terrestrial carbon pools (surface structural, surface metabolic, surface microbial, soil structural, soil metabolic, soil microbial, slow, and passive carbon pools) according to the timescale of the decomposition of carbon in each pool and transfers between different pools on the basis of the CENTURY ecosystem model [*Parton et al., 1988*] and a model of carbon exchange between vegetation, soil, and the atmosphere (CEVSA) [*Cao and Woodward, 1998*].

[14] Carbon uptake by the terrestrial vegetation-soil system is formulated as

$$\frac{\partial C_{\text{veg}}}{\partial t} = \text{GPP} - L_{\text{veg}} - R_{\text{veg}} \quad (3)$$

$$\frac{\partial C_{\text{soil}}}{\partial t} = L_{\text{veg}} - R_{\text{soil}} \quad (4)$$

where C_{veg} and C_{soil} are the carbon stored in terrestrial vegetation and soil, respectively. GPP is the terrestrial vegetation gross primary productivity calculated in the biogeophysical module, L_{veg} is the litterfall from vegetation, R_{veg} and R_{soil} are the plant autotrophic respiration and soil heterotrophic respiration, respectively. Details of the scheme are described in *Ji et al.* [2008]. The net primary productivity (NPP), which represents the net amount of CO_2 taken up by vegetation, is calculated as

$$\text{NPP} = \text{GPP} - R_{\text{veg}} \quad (5)$$

[15] From equations (3)–(4), the net ecosystem CO_2 flux can be derived as

$$\text{NEP} \equiv \frac{\partial(C_{\text{veg}} + C_{\text{soil}})}{\partial t} = \text{GPP} - R_{\text{veg}} - R_{\text{soil}} \quad (6)$$

[16] Positive value of NEP indicates net carbon uptake by the terrestrial ecosystem from the atmosphere. There is $f_{\text{land}} = -\text{NEP}$ in equation (1).

[17] The integration time step is 20 min for the photosynthesis of vegetation, 24 h for the biomass accumulation and phenological variation as well as soil carbon decomposition processes. The vegetated surfaces are divided into 15 plant functional types (PFTs) including natural vegetation and crop as the present situation. In BCC_AVIM1.0, a grid cell contains up to four PFTs which is similar to CLM3. The composition and abundance of PFTs within a grid cell are time-invariant and prescribed from 1 km satellite data [*Bonan et al., 2002*].

[18] In this study, only the land use-associated CO_2 emissions are involved in terms of E_{landuse} in equation (1). The actual land-cover changes as boundary conditions of the BCC_AVIM1.0 are not involved. Fractional land use patterns are fixed in BCC-CSM1.1 as those in 1850, therefore changes in physical and biogeochemical properties of the vegetation following actual land-cover changes are neglected.

2.3. The Oceanic Model

[19] MOM4_L40 is a global oceanic general circulation model (OGCM) with a tripolar grid of *Murray* [1996]. The horizontal resolution is 1° longitude by $1/3^\circ$ latitude between 30°S and 30°N ranged to 1° latitude at 60°S and 60°N and nominally 1° polarward with tripolar coordinates to resolve the arctic. There are 40 z -levels in the vertical. The two northern poles of the curvilinear grid are shifted to land areas over North America and Eurasia, respectively. The first 20 levels are placed between surface and 200 m depth of the upper ocean. MOM4-L40 is originated from the Z -coordinate Modular Ocean Model version 4 (MOM4) developed by the Geophysical Fluid Dynamics Laboratory (GFDL).

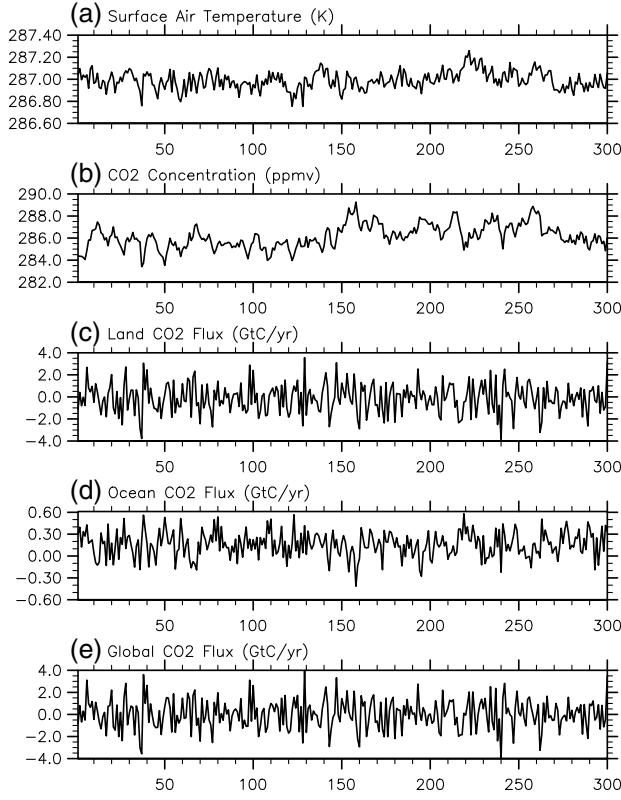


Figure 1. Time series of globally averaged annual mean of (a) surface air temperature (K), (b) CO₂ concentration (ppmv), (c) land CO₂ flux (GtC yr⁻¹), (d) oceanic CO₂ flux (GtC yr⁻¹), and (e) global CO₂ flux (GtC yr⁻¹) from the 300 year preindustrial control experiment. CO₂ fluxes are accounted positive upward.

It adopts some mature parameterization schemes in MOM4 [Griffies *et al.*, 2005], including Sweby’s tracer-based third-order advection scheme, isopycnal tracer mixing and diffusion scheme, Laplace horizontal friction scheme, KPP vertical mixing scheme, complete convection scheme, overflow scheme of topographic processing of sea bottom boundary/steep slopes, and shortwave penetration schemes based on spatial distribution of chlorophyll concentration. The biogeochemistry module to simulate the ocean carbon cycle in MOM4_L40 is based on the protocols from the Ocean Carbon Cycle Model Intercomparison Project–Phase 2 (OCMIP2, <http://www.ipsl.jussieu.fr/OCMIP/phase2/>).

[20] The OCMIP biogeochemistry module parameterizes the process of marine biology in terms of geochemical fluxes without explicit representation of the marine ecosystem and food web processes. It includes five prognostic variables: phosphate (PO₄), dissolved organic phosphorus (DOP), dissolved oxygen (O₂), dissolved inorganic carbon (DIC), and alkalinity (Alk). In OCMIP, F_{ocean} in equation (1) is calculated as

$$F_{\text{ocean}} = K_w \cdot [\text{CO}_{2\text{sat}} - \text{CO}_{2\text{surf}}] \quad (7)$$

[21] In which,

$$K_w = (1 - F_{\text{ice}}) \frac{u^2}{\sqrt{S_c}/660} \cdot 0.337 \quad (8)$$

and

$$\text{CO}_{2\text{sat}} = \alpha_c \cdot p \cdot \text{CO}_{2\text{atm}} \frac{p_{\text{sea}}}{p_{\text{atm}}} \quad (9)$$

where K_w is the gas transfer velocity [Wanninkhof, 1992], F_{ice} is the fractional sea ice cover, u is the wind speed near surface, S_c is the Schmidt’s number for CO₂ [Wanninkhof, 1992]. α_c is the CO₂ solubility for water vapor saturated air, $p \cdot \text{CO}_{2\text{atm}}$ is the partial pressure of CO₂ in dry air, p_{sea} and p_{atm} are the pressure at sea surface level and at the lowest layer of the atmospheric model, respectively. In equation (9), $\text{CO}_{2\text{surf}}$ is the surface aqueous CO₂ concentration varying in function of the oceanic surface DIC, Alk, temperature, and salinity. The DIC depends on the air-sea exchange of CO₂ and is given by

$$\frac{\partial \text{DIC}}{\partial t} = L(\text{DIC}) + Jb(\text{DIC}) + Jg(\text{DIC}) \quad (10)$$

where $L(\text{DIC})$ represents effects due to dynamic processes of advection and diffusion. $Jb(\text{DIC})$ and $Jg(\text{DIC})$ are the source/sink terms due to biological process and air-sea exchange of CO₂, respectively. $Jg(\text{DIC})$ can be written as

$$Jg(\text{DIC}) = \frac{F_{\text{ocean}}}{dz} \quad (11)$$

where dz is the top layer thickness of MOM-L40.

[22] Carbon cycle processes in MOM4-L40 are kept identical to those in OCMIP, except for parameterizing the export of organic matter from surface waters to deep oceans. This is generally known as “export production” (EP for short, also called “new production”) and is a very important process in determining the carbon cycle. In MOM4_L40, the EP is simulated with a prognostic method following Yamanaka and Tajika [1996], while the nutrient restoring approach is used in the original OCMIP. That is, the EP in MOM4_L40 is parameterized as a function of phosphate concentration,

$$\text{EP} = r \cdot L_f \cdot \text{PO}_4 \quad (12)$$

where r is a proportional factor called “bio-production efficiency” and is set to 0.8 yr⁻¹ in this work, and L_f is the light factor related to strength of the incident solar radiation [Bacastow and Maier-Reimer, 1990].

2.4. The Sea Ice Model

[23] The sea ice component of BCC_CSM1.1 is the GFDL Sea Ice Simulator (SIS). SIS is a global dynamical-thermodynamical sea ice model, where the elastic-viscous-plastic technique [Hunke and Dukowicz, 1997] is used to calculate ice internal stresses and the thermodynamics is a modified Semtner scheme from Winton [2000]. SIS has the same horizontal resolution as MOM4-L40 and three layers in the vertical, including one layer of snow cover and two layers of equally sized sea ice. In each model grid, five categories of sea ice are considered, according to the thickness of sea ice. It also takes into account the mutual transformation from one category to another under thermodynamic conditions. SIS calculates concentration,

Table 1. Globally Averaged Annual Means of CO₂ Concentration (ppmv), Land CO₂ Flux (GtC yr⁻¹), Oceanic CO₂ Flux (GtC yr⁻¹), and Global CO₂ Flux (GtC yr⁻¹) Averaged for Every 50 Years in the 300 Year Preindustrial Control Experiment^a

Years	CO ₂ Concentration (ppmv)	Land CO ₂ Flux (GtC yr ⁻¹)	Oceanic CO ₂ Flux (GtC yr ⁻¹)	Global CO ₂ Flux (GtC yr ⁻¹)
1–50	285.566	−0.168	0.167	−0.001
51–100	285.495	−0.042	0.159	0.117
101–150	285.474	−0.126	0.170	0.044
151–200	287.077	−0.074	0.110	0.036
201–250	286.823	−0.152	0.174	0.022
251–300	286.487	−0.173	0.172	0.001

^aCO₂ fluxes are accounted positive upward.

thickness, temperature, salinity of sea ice, and motions of ice sheet. More details can be found in *Winton* [2000].

2.5. Experiments

[24] The preindustrial climate state of BCC_CSM1.1 is obtained from a 300 year control simulation following the requirement of CMIP5. At first, the initial state of each component of BCC_CSM1.1 is obtained through individual “spinup” runs. The atmospheric model is integrated for 50 years forced by fixed preindustrial forcing of the year 1850, including global reconstructed SST and sea ice concentration. The land model BCC_AVIM1.0 is forced with a fixed atmospheric CO₂ concentration of 285 ppmv in 1850 and the atmospheric forcing of 1950–2000 NCEP reanalyses data in an offline way to yield a first estimate of equilibrium states for the land carbon pools. The ocean component is integrated alone for 200 years using the surface forcings from the above mentioned 50 year atmospheric integration with an atmospheric CO₂ content fixed at the value in 1850 for the OCMIP module of MOM4-L40.

[25] All components of BCC_CSM1.1 are finally fully coupled together and integrated, initiated from preindustrial conditions of the year 1850, for 100 years as “spinup,” and then 300 years control run as required by the CMIP5 [Taylor et al., 2009] to approach its quasi-equilibrium state. The globally averaged surface temperature is about 287 K (Figure 1a). The atmospheric CO₂ concentration is about 286 ppmv (Figure 1b), very close to the observed estimation of 285 ppmv for 1850.

[26] As indicated in equation (1), the atmospheric CO₂ interacts with the carbon budgets in global land and oceans. The inhomogeneous distributions of global vegetation, precipitation, and temperature cause seasonal to interannual variations of regional land carbon exchange with atmosphere, then impact on change in atmospheric CO₂ concentration. As shown in Figure 1, the atmospheric CO₂ concentration is in the range of 283 to 289 ppmv. There exist evident interannual variations of about −2.0~2.0 GtC yr⁻¹ carbon exchange between atmosphere and land and −0.2~0.4 GtC yr⁻¹ between atmosphere and ocean. If we compare Figure 1c with other model simulations such as a similar 1000 year preindustrial control experiment using the NCAR CSM1.4-carbon model in *Doney et al.* [2006], then the magnitude of variability for the global annual land CO₂ flux from BCC_CSM1.1 control run is slightly larger.

[27] In the 300 year preindustrial control experiment, the entire ocean is always, on the average, a weak carbon source, and there is a small amount of net carbon flux from ocean to atmosphere, estimated at about 0.159–0.174 GtC yr⁻¹ (Table 1) averaged for every 50 years.

At the same time, the entire land acts as a net carbon sink at about 0.042–0.173 GtC yr⁻¹ for every 50 years (Table 1). In the final 50 years of the 300 year preindustrial experiment, they are approximately balanced, only a small CO₂ flux (0.001 GtC yr⁻¹) to the atmosphere, on average (Table 1). Therefore, the BCC_CSM1.1 approaches its quasi-equilibrium state under the preindustrial condition without any anthropogenic CO₂ emission. We notice that the recent works of *Liu et al.* [2010] and *Ludwig et al.* [2011] revealed a carbon transfer of 0.24–0.60 GtC yr⁻¹ to the sea via continental rivers. This may have some influence on the carbon

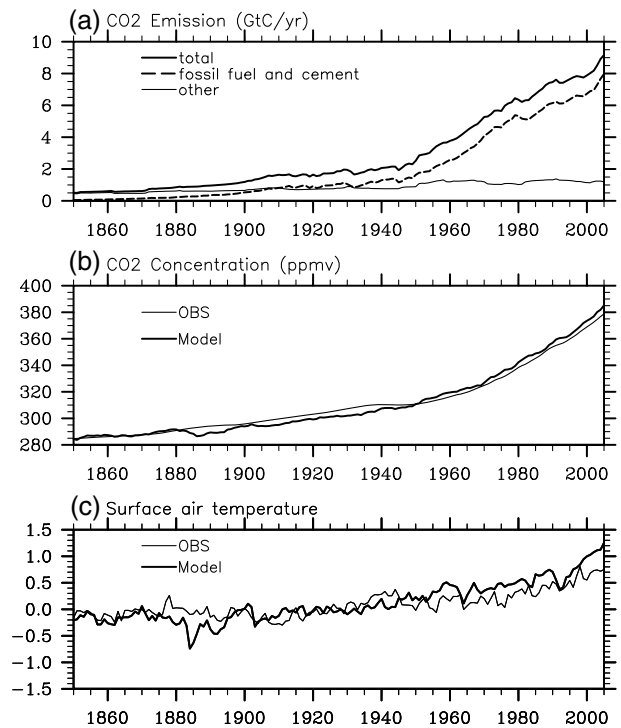


Figure 2. Time series of (a) the CMIP5-recommended global annual anthropogenic CO₂ emissions (thick solid line) due to fossil fuel combustion and cement production (dash line) and other anthropogenic activities (thin solid line), (b) the annual CO₂ concentration, and (c) the global mean surface air temperature anomalies from the historical experiment (widen solid line) compared to observations (thin solid line). The units are (a) GtC yr⁻¹, (b) ppmv, and (c) K, respectively. The observation data in Figures 2b and 2c are the CMIP5-recommended global CO₂ observation data set and the HadCRUT3 data set [Brohan et al., 2006], respectively.

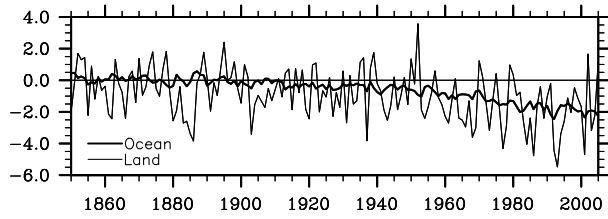


Figure 3. Time series of the simulated annual mean CO₂ flux averaged for the global ocean (thick line) and global land (thin line). The units are GtC yr⁻¹, accounted positive upward.

budget in the ocean, and even possibly to partly offset the BCC_CSM1.1 simulated net carbon source in the ocean, but it is not included in the BCC_CSM1.1.

[28] The steady state of BCC_CSM1.1 after the preindustrial control experiment is used as the initial condition for the historical experiment. The model is integrated from 1850 to 2005 with the CMIP5 recommended prescribed historical CO₂ emissions including that from fossil fuel burning and other associated with historical land use changes [Meinshausen *et al.*, 2011]. The simulation also includes all other prescribed historical forcing such as insolation, orbital forcing, tropospheric and stratospheric sulfates, volcanic aerosol, ozone, and non-CO₂ greenhouse gases like CH₄, N₂O, CFC-11, and CFC-12. All of these

forcing data are downloaded from CMIP5 website (http://cmip-pcmdi.llnl.gov/cmip5/data_portal.html).

3. Results

3.1. Performance in Simulating the Global Warming in the Last Century

[29] The ability to reproduce the global warming in the 20th century is a key point for a climate-carbon cycle model. According to the CMIP5 protocol, as shown in Figure 2a, the globally integrated anthropogenic CO₂ emission is 0.5 GtC yr⁻¹ in year 1850. It persistently increases year by year thereafter, mainly due to increase of CO₂ release from fossil fuel burning and cement production. The total anthropogenic CO₂ emission reaches about 2 GtC yr⁻¹ around 1950, and its increase is accelerated afterwards. Up to year 2000, the global total anthropogenic emission reaches about 8 GtC yr⁻¹.

[30] Under the forcing of anthropogenic carbon emissions (Figure 2a), BCC_CSM1.1 can well reproduce the atmospheric CO₂ concentration and its time evolution. As shown in Figure 2b, the simulated atmospheric CO₂ increase is in close agreement with CMIP5 recommended values (based on observations) from 1850 to 2005. The simulated atmospheric CO₂ concentration started from 286 ppmv in 1850 and increased to 385 ppmv by 2005 (Figure 2b), and the discrepancy between the simulation and observation is smaller than 10 ppmv. There is a systematic underestimate

Table 2. Global Carbon Budgets From BCC_CSM1.1 and Other Estimates for the 1980s, 1990s, and 1850–1998.

		1980s (GtC yr ⁻¹)	1990s (GtC yr ⁻¹)	1850–1998 (GtC)
Fossil fuel, cement, and biofuel emissions	Forcing data	5.2	6.0	249
	Forcing data	1.5	1.6	146
Land use emissions	BCC_CSM1.1	3.1	3.6	182
	Other estimates	3.3 ± 0.2 ^a	3.3 ± 0.2 ^a	176 ± 10 ^a
		3.1 ^d	3.4 ^d	170 ^d
		3.3 ⁱ	3.7 ⁱ	172 ^j
		3.3 ± 0.1 ^h	3.2 ± 0.1 ^h	
Ocean uptake	BCC_CSM1.1	1.6	1.8	77
	Other estimates	1.7 ± 0.6 ^b	2.4 ± 0.7 ^b	120 ± 50 ^b
		2.2 ^d	2.6 ^d	132 ^d
		1.8 ⁱ	2.2 ⁱ	
		1.9 ± 0.6 ^c	1.7 ± 0.5 ^c	
		1.8 ± 0.3 ^f	2.3 ± 0.2 ^f	
		1.96 ± 0.07 ^g	2.24 ± 0.07 ^g	
Land uptake	BCC_CSM1.1	1.8 ± 0.8 ^h	2.2 ± 0.4 ^h	
	Other estimates	2.0	2.2	136
		2.4 ± 1.1 ^c	2.9 ± 1.1 ^c	126 ± 80 ^c
		2.3 ^d	2.7 ^d	135 ^d
		2.2 ⁱ	2.6 ⁱ	
		2.2 ± 0.9 ^e	3.0 ± 1.1 ^e	
		2.2 ± 0.9 ^f	2.6 ± 0.9 ^f	
		2.18 ± 0.25 ^g	2.01 ± 0.25 ^g	
	1.7 (3.4 to -0.2) ^h	2.6 (4.3 to 0.9) ^h		

^aFrom Bolin and Sukumar [2000];

^bFrom Plattner *et al.* [2002];

^cFrom Houghton [2003];

^dFrom Matthews *et al.* [2005];

^eIPCC TAR [Prentice *et al.*, 2001];

^fRoedenbeck *et al.* [2003];

^gRaddatz *et al.* [2007];

^hIPCC AR4 [Denman *et al.*, 2007];

ⁱEby *et al.* [2009];

^jEstimated from CMIP5-recommended CO₂ observation data in this work.

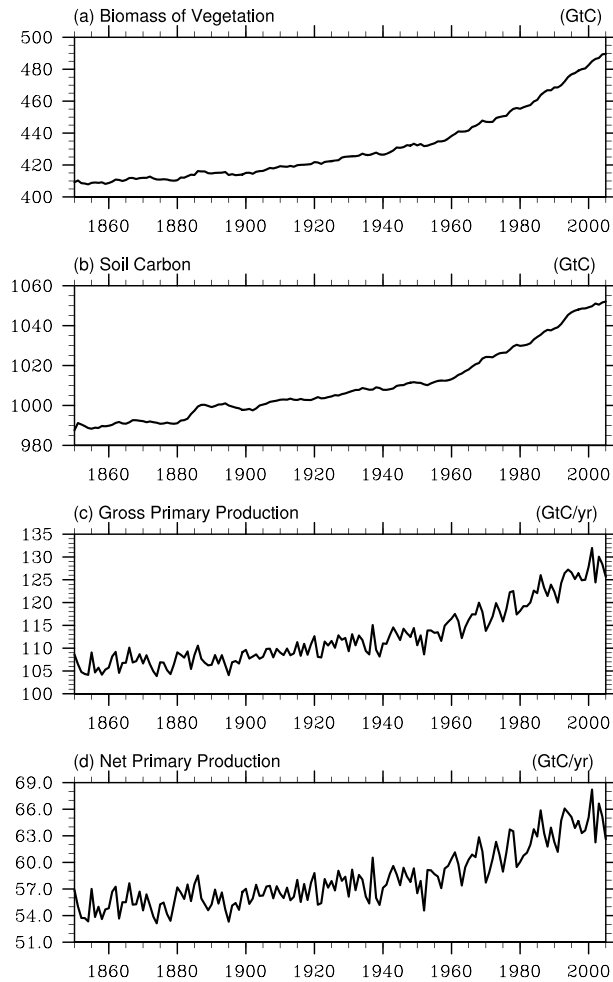


Figure 4. Time series of global annual mean of (a) vegetation biomass, (b) soil carbon, (c) gross primary production, and (d) net primary production from the historical experiment. The units are GtC in Figures 4a and 4b, and GtC yr⁻¹ in Figures 4c and 4d, respectively.

of CO₂ in BCC_CSM1.1 from 1880 to 1950, which also exists in other model studies [e.g., Matthews *et al.*, 2005; Eby *et al.*, 2009; Arora *et al.*, 2009; Murakami *et al.*, 2010]. In the latter half of the 20th century, the simulated CO₂ concentration in BCC_CSM1.1 is, however, overestimated by 5–10 ppmv relative to the observation.

[31] With the increase of atmospheric CO₂ concentration and all other historical forcing data including solar activity, aerosol, ozone, and non-CO₂ greenhouse gases, the global warming during the 20th century in BCC_CSM1.1 is well simulated (Figure 2c). Globally averaged surface air temperature (SAT) from 1850 to 2005 displays similar time evolution as the observation from HadCRUT3 SAT data set [Brohan *et al.*, 2006], with a well-reproduced long-term increasing trend of SAT. Our simulated 0.7°C increase during 1850–1995 is in good agreement with the IPCC AR4 estimate of 0.6°C ± 0.2°C [Trenberth *et al.*, 2007]. But in the last period from 1996 to 2005, the global SAT experiences a jump of 0.6°C in the model and is obviously warmer than in the observation.

[32] It is noted that the simulated SAT in some time periods such as in the 1880s, 1890s, 1900s, 1960s, and 1990s

has an evident global cooling shock. These are coincident to several significant volcanic eruptions such as Krakatoa (in 1883), Pelee (in 1902), West Indies Agung (in 1963), and Mount Pinatubo (in 1991). Each of these volcanic eruptions may lead to a significantly enhanced stratospheric aerosol optical depth (available from <http://data.giss.nasa.gov/modelforce/strataer/>). As shown in Figure 2c, the global surface air temperature may decrease by up to 0.4°C within 1 to 2 years after a volcanic eruption. This volcano aerosol response is slightly stronger than the ensemble simulation of other CMIP5 models (not shown).

3.2. Variation of Global Carbon Budget

[33] Carbon uptake by global land and ocean plays an important role in slowing down the carbon accumulation in the atmosphere. Figure 3 presents CO₂ fluxes simulated by BCC_CSM1.1 for global land and ocean, respectively. Negative values indicate fluxes from atmosphere to land or ocean. Along with the increase of anthropogenic CO₂ emission to the atmosphere (Figure 2a) especially after 1950, there is an obvious negative tendency in the second half of the 20th century for both land and ocean CO₂ fluxes (Figure 3). This decreasing slope with time indicates that the ability of carbon uptake by land and ocean are both enhanced.

[34] As a result of carbon absorption by land and ocean, part of CO₂ released by human activity stays in the atmosphere. As listed in Table 2, there are 249 GtC of CO₂ release from fossil fuel burning and 146 GtC of other CO₂ emission to the atmosphere from 1850 to 1998. During the same period, there are 136 and 77 GtC absorbed by the global land and ocean, respectively. Therefore, approximately 46% of the total 395 (i.e., 183) GtC of anthropogenic CO₂ emissions still remains in the atmosphere in BCC_CSM1.1 simulation. This leads to increase in model atmospheric CO₂ from 285 ppmv in 1850 to 369 ppmv in 1998.

[35] It is noted that the averaged ocean carbon uptakes during the 1980s and 1990s are 1.7 and 1.8 GtC yr⁻¹, respectively. They are slightly smaller than most of the previous estimates [Plattner *et al.*, 2002; Matthews *et al.*, 2005; Prentice *et al.*, 2001; Roedenbeck *et al.*, 2003; Raddatz *et al.*, 2007; Meehl *et al.*, 2007; Eby *et al.*, 2009]. However, McNeil *et al.* [2003] pointed out that most ocean general circulation models overestimated their anthropogenic CO₂ uptake over the past 2 decades. With a technique based on global chlorofluorocarbon data, the ocean net uptake was estimated 1.6 GtC yr⁻¹ for the 1980s and 2.0 ± 0.4 GtC yr⁻¹ for the 1990s, respectively. BCC_CSM1.1 is close to these results in McNeil *et al.* [2003]. Note that a consensus result for the 1990s given in IPCC-AR4 WG1 Ch7 [Denman *et al.*, 2007] is 2.2 GtC yr⁻¹.

[36] The total land CO₂ uptake simulated by BCC_CSM1.1 is, on average, 2.0 and 2.2 GtC yr⁻¹ during the 1980s and 1990s, respectively, within the previous estimated uncertainty range [Houghton, 2003; Matthews *et al.*, 2005; Prentice *et al.*, 2001; Roedenbeck *et al.*, 2003; Raddatz *et al.*, 2007; Denman *et al.*, 2007; Eby *et al.*, 2009].

[37] The carbon uptake by land is, to a large extent, determined by vegetation and soil carbon storages. Figure 4 shows

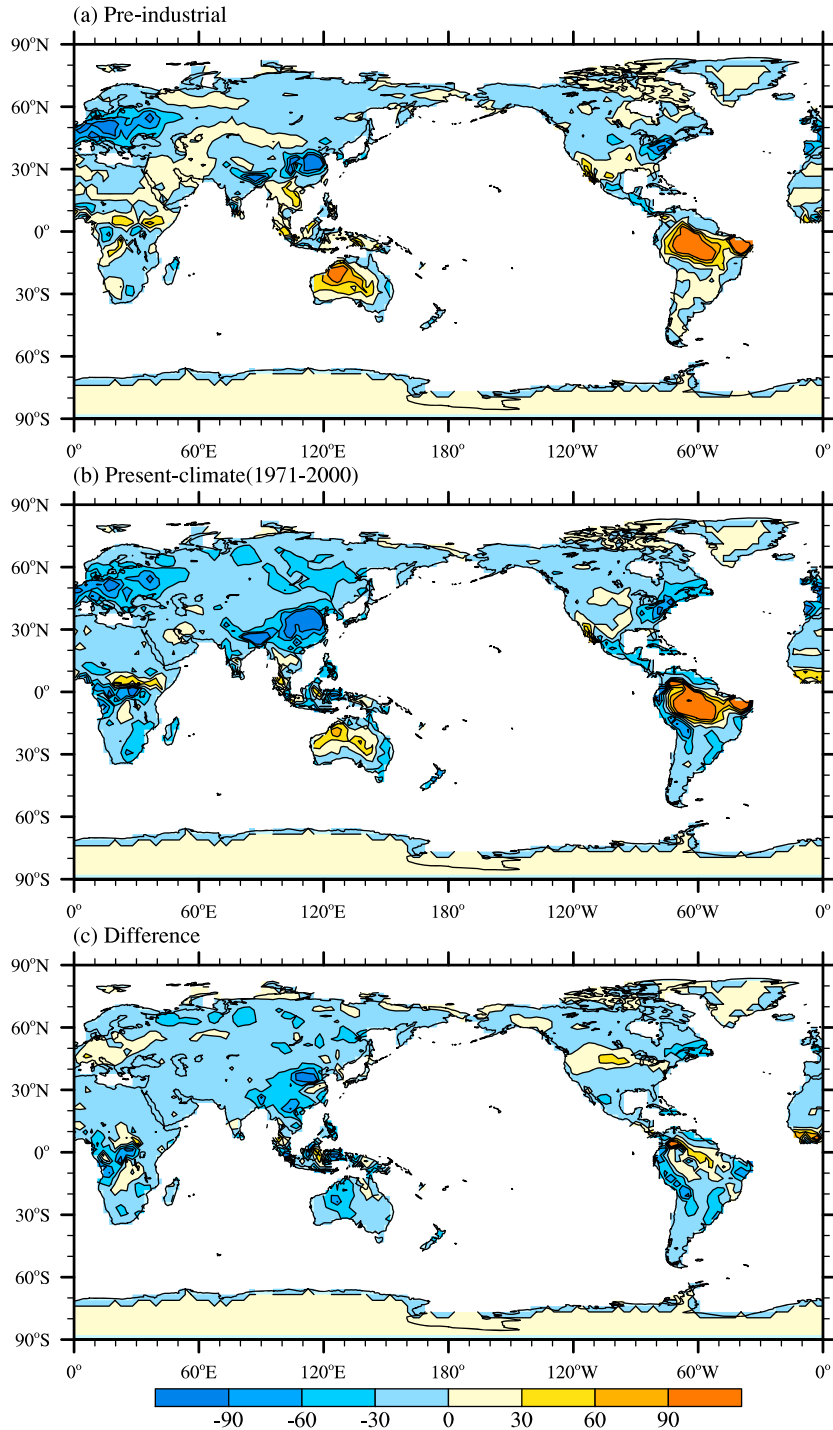


Figure 5. Geographical distribution of annual mean CO₂ net flux (accounted positive upward, from land to atmosphere) for (a) the last 30 years in the preindustrial experiment, (b) the present climate (1971–2000) in the historical experiment, and (c) the difference between Figures 5b and 5a. The units are g C m⁻² yr⁻¹.

temporal evolution of the global vegetation biomass, soil carbon storage, GPP, and NPP simulated by BCC_CSM1.1. From 1850 to 1994, the global carbon storage in vegetation increases from 410 to 470 GtC and storage in soil increases from 990 to 1046 GtC. There is a total of 116 GtC increase of carbon storage in the global land within about 150 years.

It is a little larger than the estimate of 101 GtC increase during the period of 1800 to 1994 from IPCC AR4 [Denman *et al.*, 2007] but smaller than the 128 GtC simulated by Eby *et al.* [2009]. Recent studies using satellite remote sensing data indicated that the net primary production (NPP) has increased globally over the past 2 decades [Nemani *et al.*,

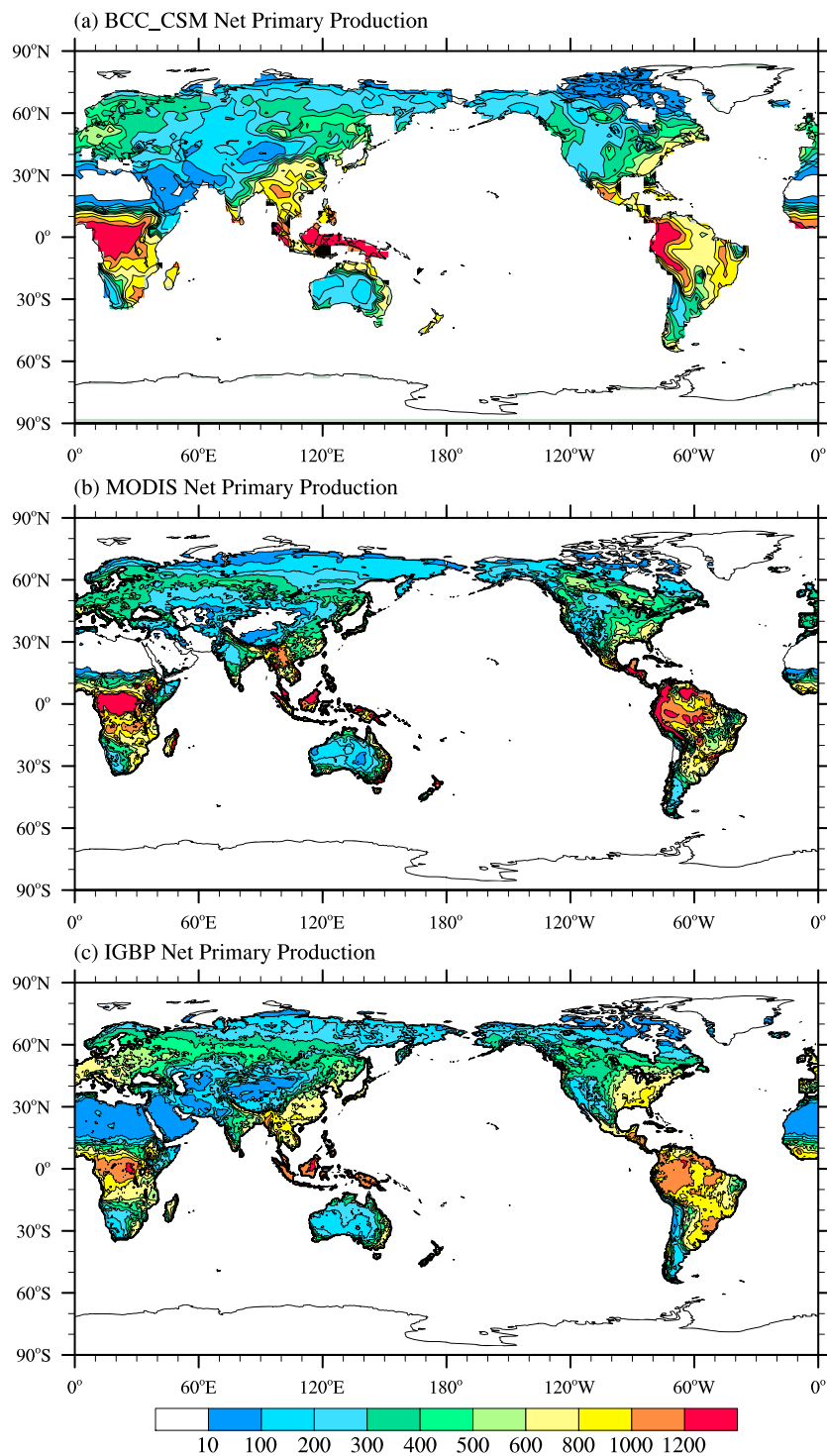


Figure 6. Geographical distribution of annual mean net primary production (a) from BCC-CSM1.1 (1971–2000 mean), (b) derived from available MODIS data (2000–2003 mean), and (c) from IGBP data. The units are $\text{g C m}^{-2} \text{yr}^{-1}$.

2003; Potter *et al.*, 2003]. As shown in Figures 4c and 4d, the simulated global annual GPP and NPP through the 20th century increase from 105 to 130 GtC and from 55 to 65 GtC, respectively. The annual mean global GPP and NPP averaged for the period of 1980 to 2000 are about 125 and

64 GtC, respectively, which are close to other observation or model-based estimates of the global GPP (125~139.7 GtC) [Zhao *et al.*, 2006; Arora *et al.*, 2009] and NPP (56.6~71.1 GtC) [Running *et al.*, 2004; Piao *et al.*, 2009a; Arora *et al.*, 2009]. However, the BCC model estimate of

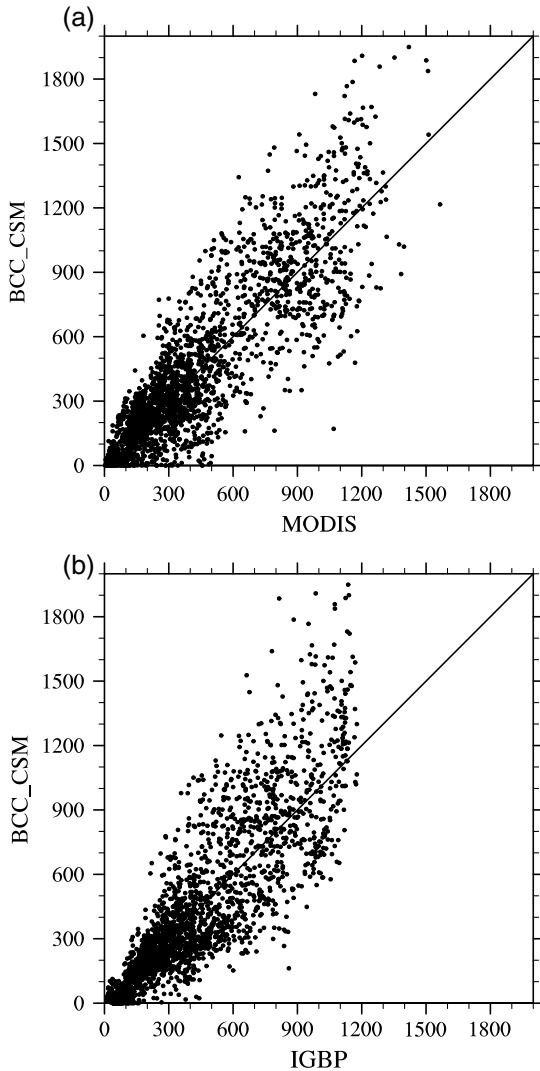


Figure 7. Scatter plots comparing annual mean NPP between (a) the BCC-CSM and MODIS, and (b) between BCC-CSM and IGBP. MODIS and IGBP data were firstly interpolated to the mesh of BCC-CSM. Each spatial grid corresponds to a point in the plots. The units are $\text{g C m}^{-2} \text{yr}^{-1}$.

GPP is significantly lower than the recent observational estimates of $150\sim 175 \text{ pgC}$ [Welp *et al.*, 2011] and $127\sim 166 \text{ pgC}$ from atmospheric CO_2 data assimilation efforts [Koffi *et al.*, 2012]. We also note that the simulated soil carbon stock as shown in Figure 4b is smaller than most of other estimates of $1220\sim 2200 \text{ pgC}$ [e.g., Sombroek *et al.*, 1993; Kimble *et al.*, 1990; Batjes, 1996]. The underestimate is possibly due to the small stock of slowly evolved passive soil carbon pool in BCC-CSM. In addition, a large amount of carbon captured in permafrost regions is not considered in BCC-CSM1.1.

3.3. Geographical Distribution

[38] Figure 5 shows the geographic distribution of the annual mean CO_2 flux averaged for the last 30 years in the preindustrial experiment and 30 years (1971–2000) in the

historical experiment. Regions of major carbon sinks or sources in the 20th century (Figure 5b) are roughly same as those in the preindustrial period (Figure 5a). Eastern U.S., China, and Europe are simulated as regions of significant carbon sink and are consistent with recent estimates from observations in Piao *et al.* [2009b]. Simulated large carbon sources to the atmosphere are located in central to western Australia, and in the central Amazon. Referring to the natural condition of the preindustrial (Figure 5a), large increases of land carbon uptake in the last 30 years of the 20th century are distributed in central Australia, coastal regions in South America continent, tropical regions, China, eastern coasts of U.S., and high-latitude regions in Russia (Figure 5c).

[39] Raddatz *et al.* [2007] showed that tropical regions play a key role in controlling the global carbon-climate positive feedback with simulations from C⁴MIP. The Amazon contains more than half of the world's tropical rain forests. Some numerical modeling studies [e.g., Prentice and Lloyd 1998] and empirical studies [Malhi *et al.*, 1998] suggested that tropical forests are terrestrial carbon sinks, but recent studies indicated that the sink of tropical Americas is rather weak [Malhi, 2010] or even a source of CO_2 when deforestation is taken into consideration [Pan *et al.*, 2011]. As indicated by equation (6) in section 2.2, the carbon exchange between land and atmosphere in the Amazon tropical forest is represented as a small difference of two large terms: the gross fluxes of NPP and the soil respiration, therefore, determination of carbon sink or source is a delicate operation.

[40] Figure 6 presents the spatial distribution of the 1971–2000 averaged annual mean NPP from BCC_CSM historical simulation, as well as results from Moderate Resolution Imaging Spectroradiometer (MODIS) data for 2000–2003 and from the International Geosphere-Biosphere Programme (IGBP) Global NPP Model Intercomparison Data. The annual mean IGBP NPP data were obtained from the Website of International Satellite Land Surface Climatology Project Initiative II (ISLSCP II) which comprises 17 global models with biogeochemistry [Cramer *et al.*, 1999]. We can see that tropical forests in BCC_CSM1.1 contain a large amount of live biomass. Tropical regions see the largest NPP, and boreal forest regions experience the second largest NPP. These results are quite consistent with MODIS and IGBP data. In the Amazon region ($50\sim 70^\circ \text{W}$, $10\sim 20^\circ \text{S}$), the NPP from BCC model simulation, MODIS, and IGBP estimates accounts for 6.6%, 9.4%, and 8.8% of the global NPP, respectively. Simulated values of NPP in Western Europe, Eastern China, and the southeastern United States are larger than the counterparts in MODIS, but slightly lower than those from IGBP data. The above three regions are all crop fields where a large uncertainty exists in photosynthesis parameterization for crops in climate models. Figure 7 presents scatter plots of NPP as shown in Figure 6 for global grid points from BCC_CSM1.1 and MODIS, and from BCC_CSM1.1 and IGBP. On average, BCC_CSM1.1 is relatively larger than MODIS, especially for high NPP above $0.6 \text{ kg C m}^{-2} \text{yr}^{-1}$. It is closer to IGBP but the maximum of NPP is limited below $1.2 \text{ kg C m}^{-2} \text{yr}^{-1}$.

[41] As shown in Figure 6, the maximum model bias comparing with MODIS and IGBP data is located in South America. The simulated NPP in the central part of the Amazon is approximately $0.6\sim 1.2 \text{ kg C m}^{-2} \text{yr}^{-1}$, which is

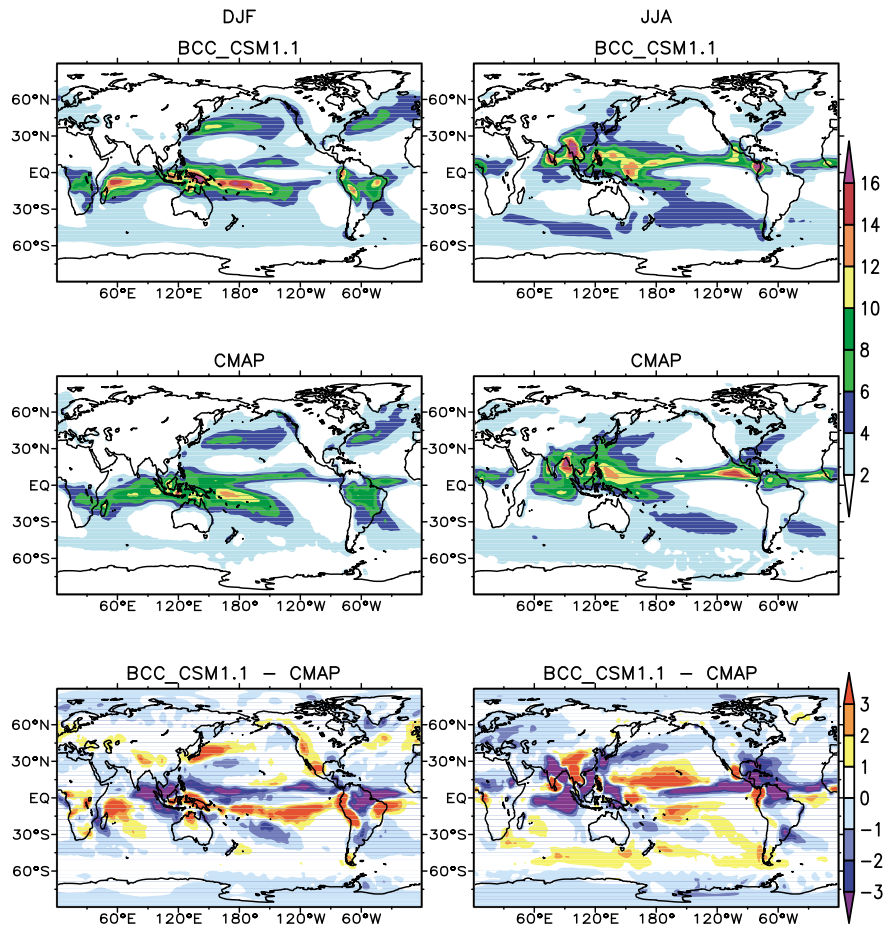


Figure 8. The 1979–2000 averaged mean precipitation of (left) December–January–February (DJF) and (right) June–July–August (JJA) from (top) BCC_CSM1.1 and (middle) the CMAP observation, and (bottom) their difference. The units are mm d^{-1} .

smaller than the estimations derived from MODIS and IGBP data. It is also smaller than estimates about $1.15 \text{ kg C m}^{-2} \text{ yr}^{-1}$ in *Senna et al.* [2009] and $1.273 \sim 1.350 \text{ kg C m}^{-2} \text{ yr}^{-1}$ in *Nunes et al.* [2012]. This discrepancy is probably caused by insufficient precipitation in the Amazon simulated in BCC_CSM1.1. As presented in Figure 8, the overall patterns of the mean precipitation for December–January–February (DJF) and June–July–August (JJA) from BCC_CSM1.1 resemble their counterparts in observations. The domains covered by larger than 4 mm d^{-1} are approximately coincident with the observation. The areas with high rainfall in DJF from CPC (Climate Prediction Center) Merged Analysis of Precipitation (CMAP) data over the western parts of the southern tropical Pacific, the southern tropical Indian Ocean, South Africa, and South America, except a weak rain belt over the northern tropical Pacific near the equator, are all well captured by BCC_CSM1.1. The secondary maxima of precipitation over midlatitudes are also reasonably reproduced. In boreal summer (JJA), high rainfall is mainly distributed along the equatorial Pacific and the Asian summer monsoon area and is well reproduced by BCC_CSM1.1. However, remarkable regional negative biases of precipitation from BCC_CSM1.1 exist in the Amazon for both DJF and JJA. This model bias of insufficient precipitation in the Amazon also exists in austral autumn and spring (not shown).

[42] Figure 9 presents the annual mean air-sea CO_2 fluxes averaged over 30 years for the 300 years preindustrial experiment and present-day climate (1971–2000) of the historical experiment. Main spatial patterns for both preindustrial (Figure 9b) and 20th century (Figure 9a) are quite similar to the estimate of *Takahashi et al.*, [2009] (Figure 9d). All the three panels in Figure 9 are characterized by outgassing of CO_2 to the atmosphere from the equatorial Pacific and Atlantic, and by oceanic uptake at high latitudes of the two hemispheres. In the north Pacific and north Atlantic, there are large carbon uptake regions. The intensity and location of those carbon sources or sinks from the observational estimates of *Takahashi et al.* [2009] are well simulated by BCC_CSM1.1. Comparing with the observational estimate, a large discrepancy is found in the Southern Ocean. Some studies have shown the Southern Ocean south of 40°S to be a large sink for anthropogenic CO_2 [*Sarmiento and Sundquist*, 1992; *Sarmiento et al.*, 1998; *Russell et al.*, 2006; *Ito et al.*, 2010]. But as shown in Figure 9a, the Southern Ocean acts as a natural carbon sink except in a narrow belt of carbon source around $45\text{--}60^\circ\text{S}$ in BCC_CSM1.1. Such a region of weak CO_2 source also exists in observational estimates of *Takahashi et al.* [2009].

[43] If we take the natural condition of the preindustrial (Figure 9b) as a reference, the variation of oceanic carbon exchange (Figure 9c) from preindustrial to present-day

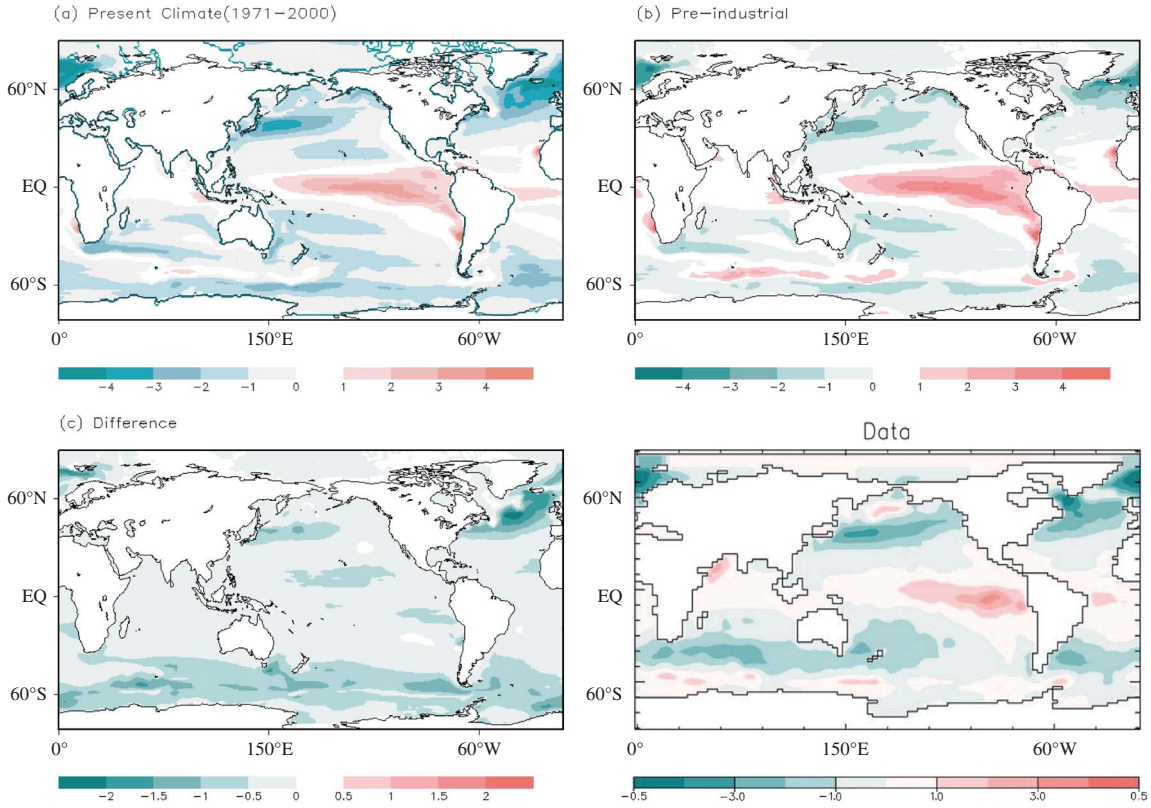


Figure 9. Annual mean air-sea CO₂ fluxes from (a) the historical simulation in 1971–2000, (b) the preindustrial simulation (last 30 years), and (c) the difference between Figure 9a and 9b, and (d) observational estimates (from *Eby et al.* [2009]; originated from *Takahashi and Coauthors* [2009]). Negative values denote ocean uptake, and the units are mol m⁻² yr⁻¹.

climate is dominated by strong carbon uptakes in higher latitudes, especially in the North Atlantic and the Southern Ocean.

[44] Figure 10 shows the net annual carbon fluxes to the atmosphere for different latitudinal zones from 1850 to 2005. BCC_CSM1.1 indicates moderate carbon sources in the tropics and carbon sinks in other latitudinal zones. The largest sink is located in northern midlatitudes, which is generally in agreement with other simulation results [e.g., *Tans et al.*, 1990; *Gurney et al.*, 2002] and estimates from CO₂ vertical profiles measures [*Stephens et al.*, 2007]. The midlatitude Southern Ocean shows a weak carbon source before 1910 but thereafter begins to weaken and gradually shifts to a weak carbon sink. In most areas of the northern hemisphere, an increase in ability of carbon uptake starts from 1960, and in the tropics, a decrease of the carbon source occurs at almost the same time. But a notable increase in the ability of carbon uptake over the Southern Ocean starts since 1980s.

3.4. Interannual to Long-Term Variation for the Recent 50 Years

[45] Table 3 lists the net carbon fluxes over land and ocean for four different latitudinal belts (as defined in *Piao et al.* [2009a]). In the last 50 years of the 20th century, the tropics still acts as a weak carbon source, and there is a flux of

0.43 GtC yr⁻¹ (to the atmosphere) in the last decade of the 20th century, with main contributions from the tropical oceans (0.53 GtC yr⁻¹). The other three zones show increasing trends of carbon sink. The northern midlatitude land (20°N–50°N) and the Southern Ocean (south of 20°S) are regions of relative strong carbon sink. In the 1990s, the carbon flux is -1.22 GtC yr⁻¹ in northern midlatitude, and -1.29 GtC yr⁻¹ in the Southern Ocean, respectively. The total land carbon uptake is enhanced from 0.41 GtC yr⁻¹ in the

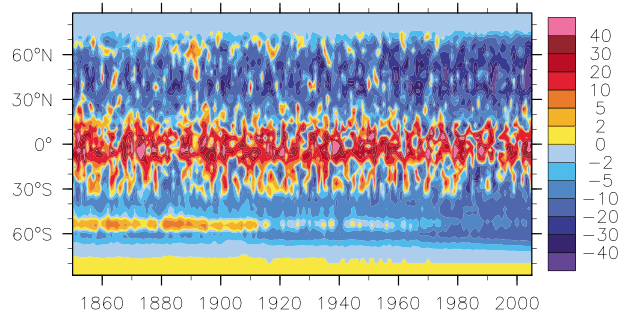


Figure 10. Time latitude diagram of zonally averaged annual mean CO₂ fluxes from the historical experiment. Units: gC yr⁻¹.

Table 3. Net Carbon Fluxes (Accounted Positive Upward) for Different Latitudinal Zones and Different Time Periods^a

Latitudinal Zone		Preindustrial	1950s	1960s	1970s	1980s	1990s
50°N–90°N	L	-0.22	-0.52	-0.57	-0.52	-0.69	-0.71
	O	-0.17	-0.24	-0.25	-0.25	-0.29	-0.29
	L+O	-0.39	-0.75	-0.82	-0.78	-0.98	-1.00
20°N–50°N	L	-0.64	-0.53	-1.42	-1.16	-1.11	-1.22
	O	-0.45	-0.62	-0.67	-0.70	-0.77	-0.78
	L+O	-1.09	-1.16	-2.09	-1.86	-1.88	-2.01
20°N–20°S	L	0.58	0.66	-0.13	0.28	0.24	-0.10
	O	1.16	0.92	0.77	0.71	0.62	0.53
	L+O	1.74	1.57	0.64	0.99	0.86	0.43
20°S–90°S	L	0.11	-0.02	-0.09	0.19	-0.41	-0.17
	O	-0.37	-0.77	-0.83	-1.04	-1.21	-1.29
	L+O	-0.26	-0.78	-0.92	-0.85	-1.62	-1.45
Global flux	L	-0.17	-0.41	-2.21	-1.21	-1.98	-2.20
	O	0.17	-0.71	-0.97	-1.28	-1.65	-1.83
	L+O	0.00	-1.12	-3.18	-2.50	-3.63	-4.04
Anthropogenic emission		0.00	3.18	4.35	5.78	6.71	7.63

^aThe units are GtC yr⁻¹. “L,” “O,” and “L + O” denote the carbon flux over land, ocean, and the sum, respectively. In the preindustrial column, numbers are from the last 50 years of the preindustrial control experiment. Negative and positive values show carbon sink and source, respectively.

1950s to 2.2 GtC yr⁻¹ in the 1990s, and the global ocean carbon uptake from 0.71 GtC yr⁻¹ in the 1950s to 1.83 GtC yr⁻¹ in the 1990s.

[46] Previous studies show that interannual variability in the atmospheric CO₂ concentration is well correlated with the El Niño–Southern Oscillation (ENSO) cycle [e.g., Bacastow, 1976; Jones et al., 2001]. Figure 11a shows time series of observed annual mean Niño-3 index and natural changes in annual mean atmospheric CO₂. Their correlation coefficient from 1959 to 2005 is 0.528, significant at the 99% confidence level. The “observed” globally averaged atmospheric CO₂ concentrations are the CMIP5-recommended data and created by Meinshausen et al. [2011]. Natural variability of CO₂ concentration is estimated from its annual increment (i.e., the CO₂ concentration minus that of the year before) subtracting a linear trend that is considered as the contribution of anthropogenic emissions to atmospheric CO₂ variation. The Niño-3 index is the mean SST anomaly in the region 5°N–5°S, 150°W–90°W and downloaded from <http://www.metoffice.gov.uk/hadobs/hadisst/data/download.html>.

[47] From BCC_CSM1.1, the natural variability of annual mean atmospheric CO₂ concentration is also highly correlated with the model Niño-3 index. Their correlation coefficient is 0.426 and significant at the 95% confidence level. Jones et al. [2001] suggested that this positive correlation between the global atmospheric CO₂ and Niño-3 index can be largely attributed to climatic changes over land during El Niño events which lead to decreased gross primary productivity and increased plant and soil respiration.

[48] The close relationship between CO₂ flux and Niño3 SST (Figure 11) is mainly attributed to CO₂ variation in the tropics. Figure 12 shows a wavelet power spectrum, calculated as in Torrence and Compo [1998] after removing long-term trends of the CO₂ flux, for the time series of annual mean CO₂ flux from 1850 to 2005 averaged over three zones in the northern midlatitudes, tropics, and southern midlatitudes. These are three regions with remarkable variations for CO₂ exchanges of land-atmosphere and ocean-atmosphere (Figure 10). In Figures 12a and 12b, most of the significant power at 95% confidence level is concentrated

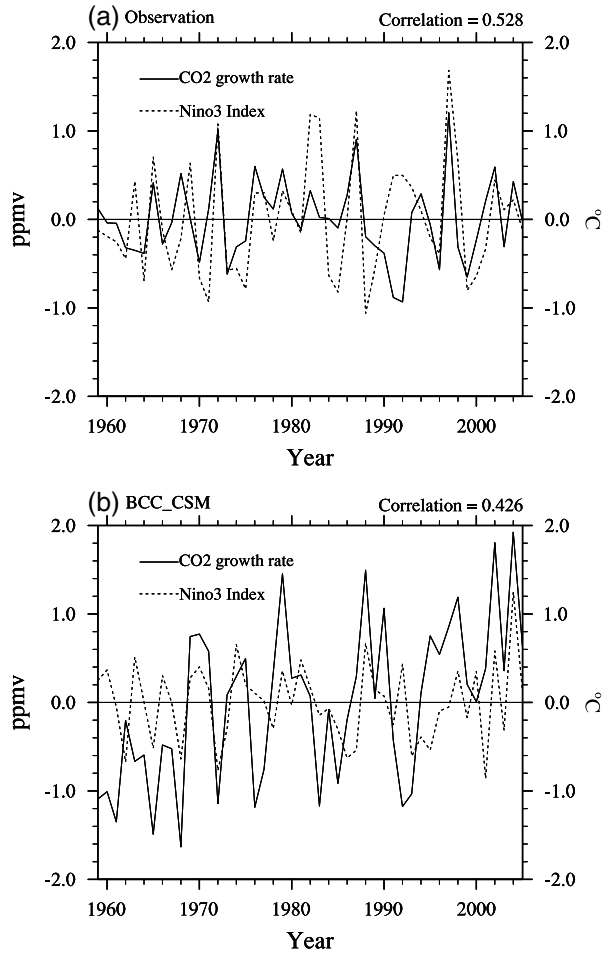


Figure 11. (a) Time series of the yearly Niño-3 index (°C) (dashed line) and the annual increment of atmospheric CO₂ (ppmv) (solid line) derived from the Hadley SST data and CMIP5-recommended CO₂ values, and (b) as in Figure 11a but from BCC-CSM1.1.

within the ENSO band of 2–8 years, although there is appreciable power at longer periods. In the tropics, there is a remarkable peak, and the largest amplitude of the wavelet

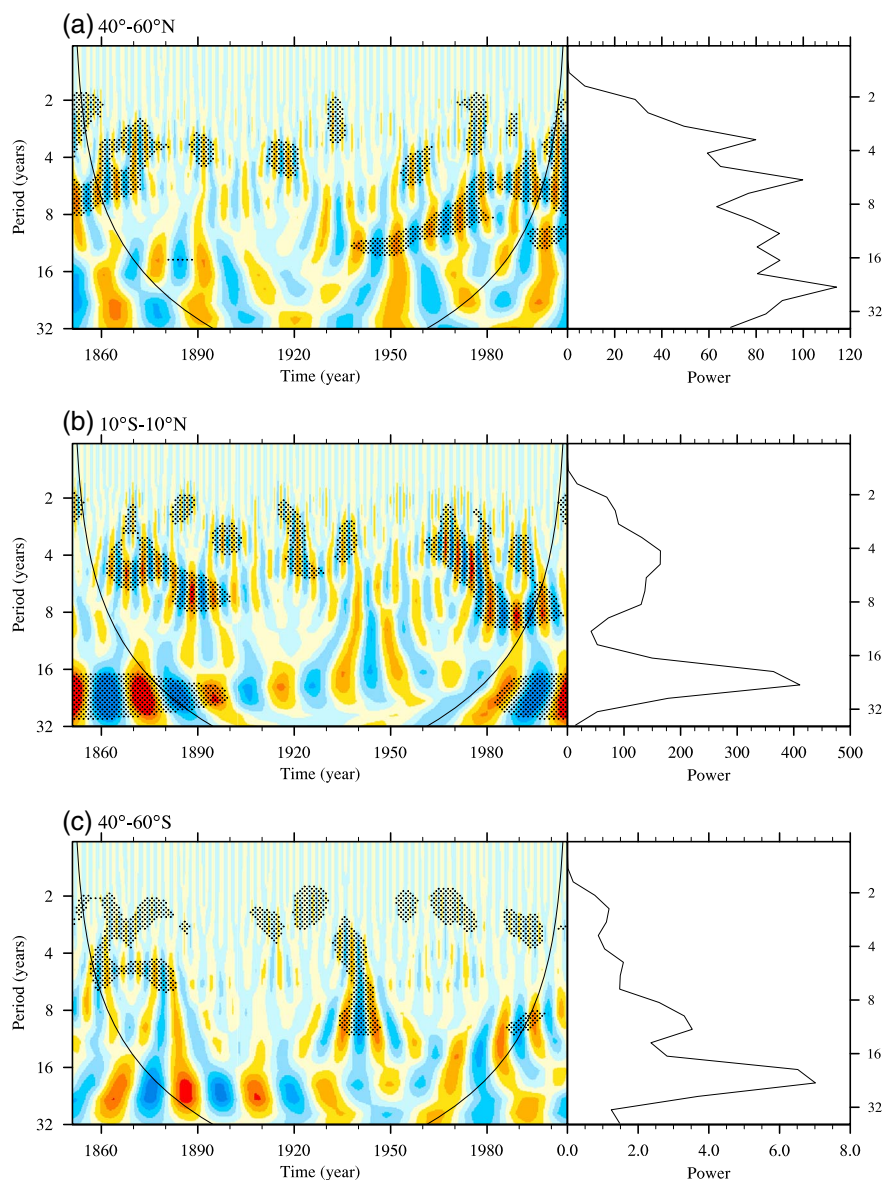


Figure 12. Morlet wavelet power spectra of the annual mean CO₂ flux from 1851 to 2005 averaged for the latitudinal zone of (a) 40°N–60°N, (b) 10°S–10°N, (c) 40°S–60°S. The cross-hatched region denotes the 95% confidence level. The right part in each panel shows integrated power over all scales and times. The left and right axes are the period (in years). The right part of horizontal axis denotes the amplitude of power spectrum (g C yr^{-1})².

power spectrum is near the cycle of 4 years. But it cannot be discerned in higher latitudes.

[49] The late half of the 20th century experiences the most rapid increase of anthropogenic carbon emission to the atmosphere and is also a period of strong carbon uptakes by ocean and land. Figure 13 presents the long-term trends of annual mean net CO₂ flux to the atmosphere from 1950 to 2000. Negative (positive) value in Figure 13 means increase (decrease) of carbon uptake or decrease (increase) of carbon emission by land and ocean. It features negative values over most areas of land including areas of major terrestrial CO₂ sinks, such as the central-eastern US, north China, and north Europe (shown in Figure 5b). It implies that the carbon uptakes by land over these areas are intensified with time. The area of large carbon source in the

Amazon (Figure 5b) is depicted as an area of remarkable negative trend in Figure 13. This denotes a weakening of carbon emission with time. There are several regions of positive trends in the northwest U.S., southern Europe, and eastern Africa (Figure 13) showing a long-term trend of weakened carbon uptake by land. Increase of oceanic CO₂ uptake is mainly distributed in higher latitudes of the North Atlantic, the Southern Ocean, and the North Pacific east to Japan (Figure 13). The main patterns for the trends of oceanic CO₂ uptake resemble other available results, such as those of the Max Planck Institute Earth System Model [Crueger *et al.*, 2008].

[50] Interannual variations of air-land carbon exchange are closely related to local air temperature and soil moisture which are the most important climate variables driving the vegetation

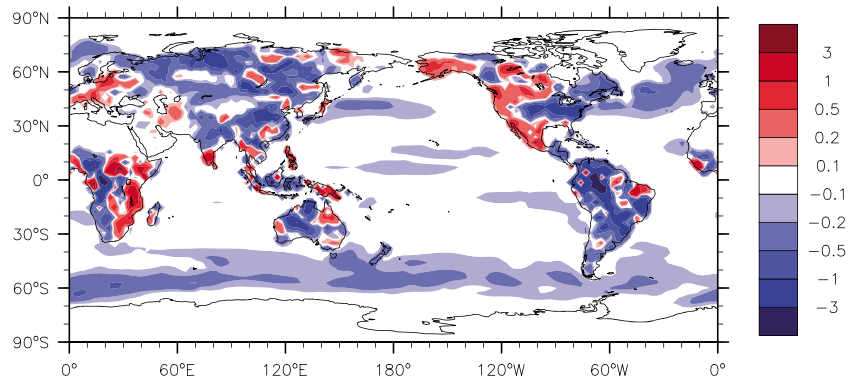


Figure 13. Linear trend (evaluated from 1951 to 2000) of the annual mean CO₂ flux at the surface (accounted positive upward) expressed as an average annual increment ($\text{g C m}^{-2} \text{yr}^{-1}$). Negative value denotes increase (decrease) of carbon uptake (emission) rate by land or ocean.

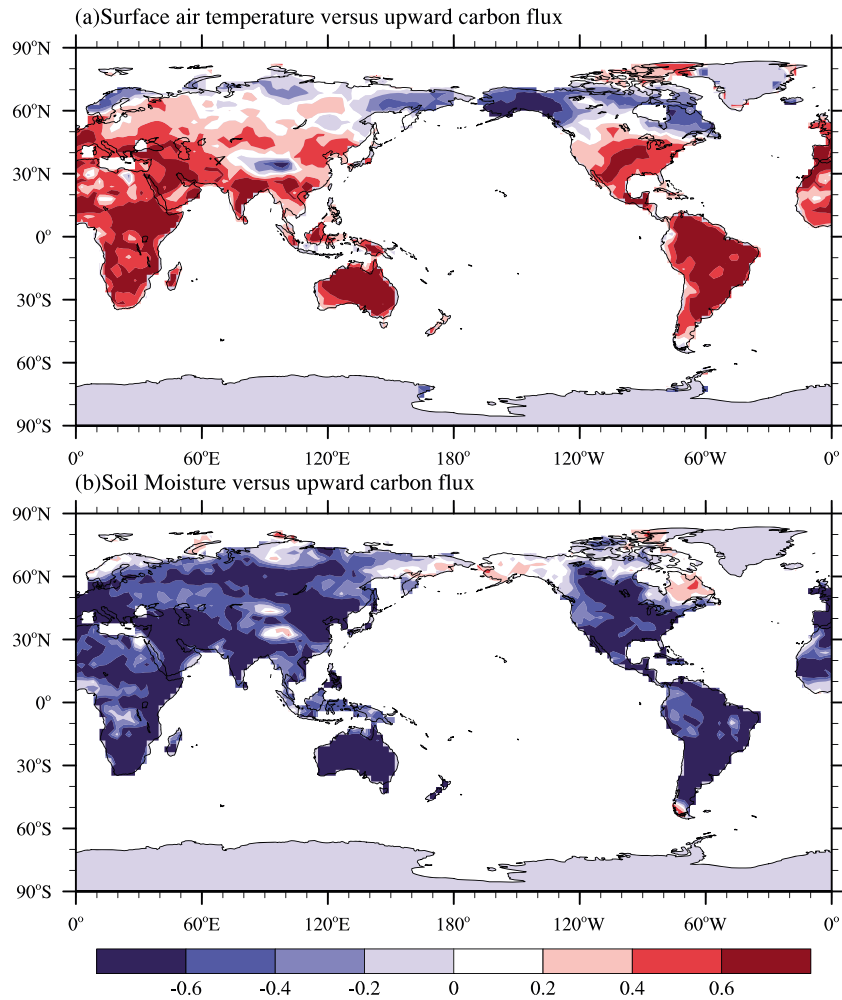


Figure 14. Temporal correlation coefficients between the annual mean net carbon flux (accounted positive from land to atmosphere) and (a) the air surface temperature, (b) the soil moisture in the 1 m layer for the period of 1951–2000 from the historical experiment. The mean trends in surface temperature, soil moisture, and carbon flux over the period of 1951–2000 are removed before calculating the correlation.

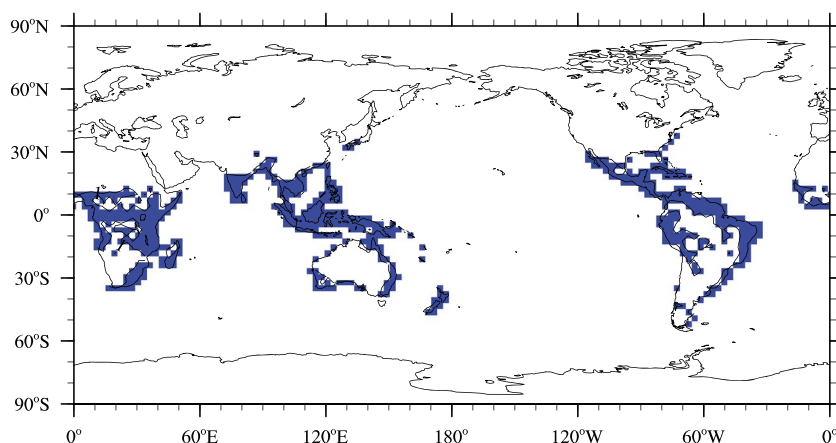


Figure 15. The colored areas show where the contribution of soil moisture to the variance of yearly averaged variation of net carbon flux from land larger than that of surface air temperature. They are results from the linear regression of yearly averaged net carbon flux with soil moisture and surface air temperature over the period of 1951–2000, and their mean trends are removed before calculating regression.

dynamics and land carbon cycle. Figure 14 shows temporal correlation coefficients of the net land-to-atmosphere carbon flux with the surface air temperature (Figure 14a) with the soil moisture (Figure 14b). A linear trend that is mainly related to the global warming is removed before calculating the correlation coefficient to focus only on the interannual timescale. Figure 14a shows clearly that the net carbon flux from land to atmosphere in low-to-midlatitudes is positively correlated with the surface air temperature. High correlation coefficients larger than +0.4 cover almost the whole continental areas between 40°S and 40°N and are significant at the 95% level. It means that the land uptake of CO₂ decreases with increased air temperature. This is due to the fact that a high air temperature can limit the photosynthesis of vegetation during their growing season while increase the soil respiration at the same time. This is coherent with the positive correlation between the soil temperature and soil respiration, found in *Savage and Davidson* [2001] and *Borken et al.* [2003]. However, in high latitudes of the northern hemisphere and over the main part of the Tibetan Plateau where climatological mean surface air temperature is low and temperature is the primary constraint on vegetation growth, an increase of air temperature is more favorable for the vegetation photosynthesis and results in an increased carbon uptake by land.

[51] The correlation between the land-to-atmosphere carbon flux and the soil moisture (Figure 14b) is almost opposite to the counterpart involving surface air temperature. Negative correlations span almost the whole land, except for the higher northern latitudes and the eastern Tibetan Plateau. The simulated land CO₂ uptake intensifies with increased soil moisture in most of the globe at interannual timescale. A plausible explanation is that a wetter soil is more favorable for the increase of NPP than for the increase of soil respiration in lowland areas. The situation is converse in high altitudes like the Tibetan Plateau. *Savage and Davidson* [2001] have shown that a drier condition resulting from climate change likely decreases soil respiration in uplands and increases in wetlands. In other words, wetter conditions can increase soil

respiration in uplands, which is consistent with the behavior of BCC-CSM1.1 over the Tibetan Plateau.

[52] Figure 15 shows relative contributions to yearly averaged net carbon flux for surface air temperature and soil moisture variations from results of linear regression. In tropical areas, soil moisture is more important than air temperature because moist soil condition is favorable for more terrestrial CO₂ uptake, while high temperature impedes vegetation growth in usually hot tropical regions. But in other parts of the globe, surface air temperature is more important to land carbon dynamics.

[53] In Figures 16–19, we present the regional mean time evolutions (from 1950 to 2000) of a few relevant variables including the surface air temperature, precipitation, soil moisture within the top 1 m layer, and the net carbon flux to the atmosphere, averaged for the Amazon tropical forest, eastern U.S., eastern China, and western Europe.

[54] The Amazon tropical forest is an old-aged tropical forest containing large stores of live biomass and soil organic matter. Net carbon source to the atmosphere in the Amazon, simulated in BCC-CSM1.1, is mainly attributed to biases of the model which result in a warm and dry soil. As shown in Figure 16a, the Amazon (20°S–10°N, 50°W–70°W) regionally averaged surface air temperature in the simulation is systematically higher than in the NCEP reanalysis by about 2–3 K. From the 1960s to 2000s, there is a slight trend of warming after 1980 in BCC_CSM1.1, which does not exist in the NCEP reanalysis. There is also a dry bias of about 1.5 mm d⁻¹ in precipitation in the Amazon in comparison to the CMAP data from 1979 to 2005 (Figure 16b). Warm temperature and less precipitation lead to dryness in the soil. As shown in Figure 16c, the Amazon regionally averaged soil moisture in BCC_CSM1.1 is about 0.11 drier than the soil moisture of 0.31–0.33 in the NCEP reanalysis. The net carbon flux to the atmosphere in the Amazon has a large interannual variation (Figure 16d), which is negatively correlated with the soil moisture at the interannual timescale (Figure 16c) with a correlation coefficient of –0.92.

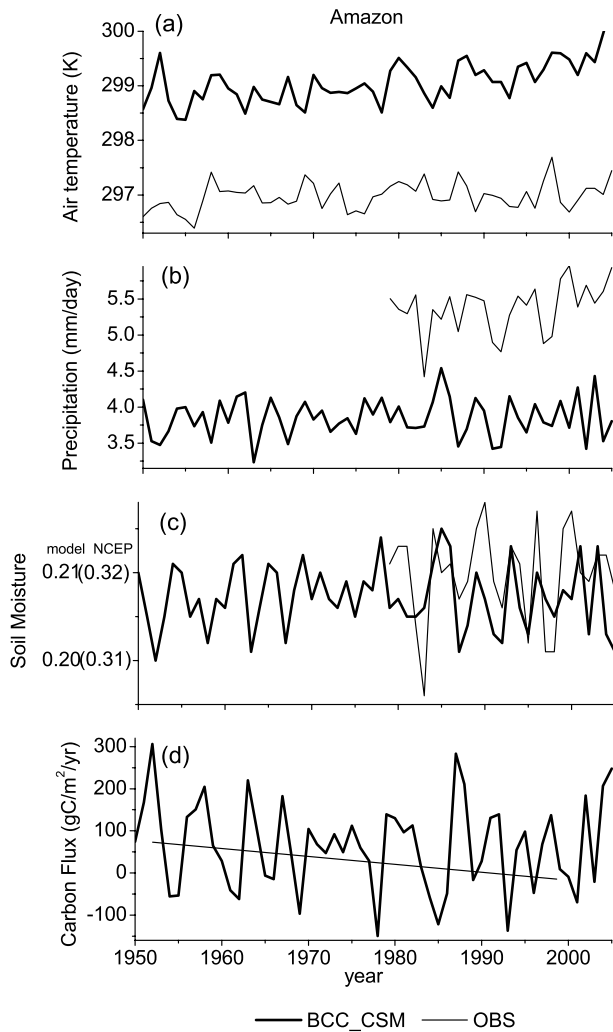


Figure 16. Annual mean time series, averaged over the Amazon (20°S – 10°N , 50°W – 70°W), for (a) surface air temperature from BCC_CSM1.1 and the NCEP reanalysis (thin solid line), (b) precipitation rate from BCC_CSM1.1 and the CMAP observation (thin solid line), (c) soil moisture in the 1 m layer from BCC_CSM1.1 and the NCEP reanalysis data (thin solid line), and (d) net CO_2 flux from land to atmosphere. The thick solid lines denote the simulation from the historical experiment. The units are (a) K, (b) mm d^{-1} , (c) g g^{-1} , and (d) $\text{g C m}^{-2} \text{yr}^{-1}$, respectively.

[55] As for the eastern U.S. (70°W – 90°W , 35°N – 45°N , Figure 17a), the observed variation of regional mean surface air temperature from 1951 to 1980 is well simulated by BCC_CSM1.1, especially the cooling trend in the 1950s. After 1980, the surface air temperature is slightly overestimated by about $1\text{--}2^{\circ}\text{C}$ by BCC_CSM1.1. In Figure 17b, the intensity of simulated precipitation is close to the CMAP data. The trend of soil moisture is also well captured in comparison with the NCEP reanalysis (Figure 17c), although the simulation is a little drier by about 0.05. Under this climate condition, the eastern U.S. is simulated as a carbon sink (Figure 17d). Our results seem coherent with Nemani *et al.* [2002] showing a trend of increasing terrestrial carbon uptake (due to increased precipitation and soil moisture) over North America.

[56] Eastern China (100°E – 120°E , 25°N – 40°N) is simulated as one of the largest carbon sink regions. As shown in Figure 18, the annual surface air temperature from the NCEP reanalysis almost falls in the range of 283 K – 285 K from 1950 to 1995, and there is an evident warming trend after 1995. This tendency is well reproduced by BCC_CSM1.1, although the simulated mean surface air temperature is generally lower than that in the NCEP reanalysis by about 2°C . The regional mean annual precipitation in BCC_CSM1.1 is systematically larger than the CMAP observation by about 1 mm d^{-1} . There is not any obvious trend from 1951 to 2005 for either BCC_CSM1.1 or CMAP. The variation of BCC_CSM1.1 simulated soil moisture is generally consistent with that in NCEP reanalysis although it is drier by about 0.02. Eastern China is a persistent carbon sink in the simulation of BCC_CSM1.1. We note however that a few recent studies showed a high vulnerability for the terrestrial ecosystem in eastern China. For example, Xiao *et al.* [2009] and Zhang *et al.* [2009] showed that severe and extended droughts can significantly affect the terrestrial carbon cycling in China and even cause the countrywide terrestrial ecosystems to switch from a carbon sink to a source.

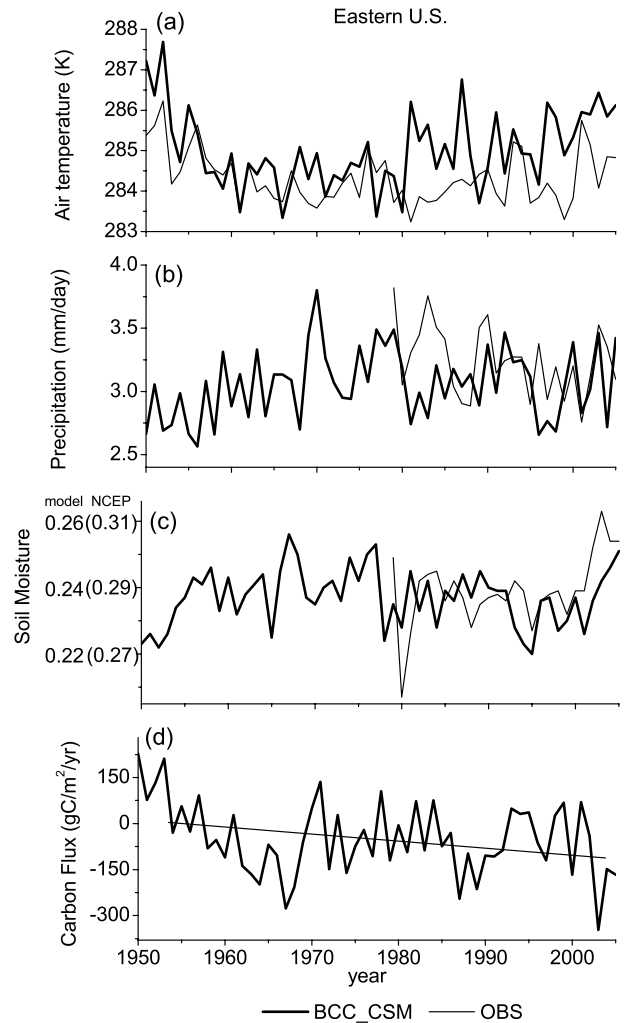


Figure 17. The same as in Figure 16 but for the regional mean in the eastern U.S. (70°W – 90°W , 35°N – 45°N).

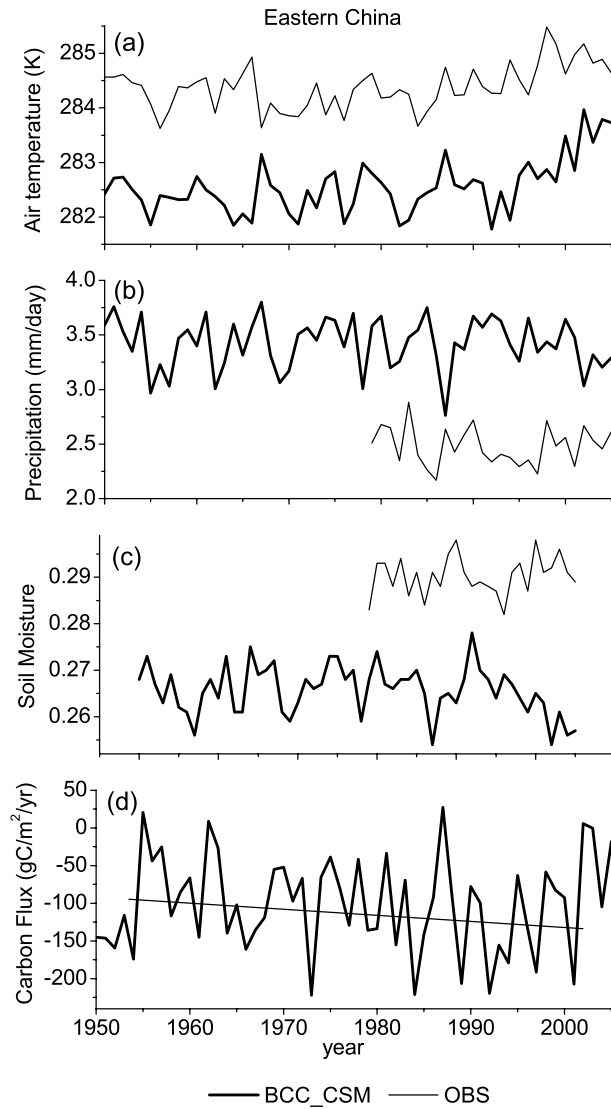


Figure 18. The same as in Figure 16 but for eastern China (100°E – 120°E , 25°N – 40°N).

[57] European ecosystems have been reported to be a carbon sink, which is estimated to be 135 – 205 GtC yr^{-1} [Janssens *et al.*, 2003], 185 – 285 GtC yr^{-1} [Schulze *et al.*, 2009], and an average of 100 GtC yr^{-1} between 1980 and 2007 [Churkina *et al.*, 2010] based on the compilation of various observations. The simulated net carbon flux to the atmosphere (Figure 19d) reveals that western Europe is a persistent carbon sink in BCC_CSM1.1, consistent with the above-cited studies. The mean flux averaged for the region (15°E – 40°E , 45°N – 60°N) is about $70 \text{ gC m}^{-2} \text{ yr}^{-1}$. There is a slight decreasing trend in the annual mean carbon uptake in the late half of the 20th century. This trend in long-term timescale partly results from the warming in the air temperature. As shown in Figure 19a, the observed warming trend of the surface air temperature from the 1960s to 2000s averaged for western Europe is well reproduced by BCC_CSM1.1. The simulation of precipitation and soil moisture from BCC_CSM1.1 is close to the CMAP observation and NCEP reanalysis. There does not exist any evident signal of increasing or decreasing tendency in precipitation and soil moisture from 1951 to 2000.

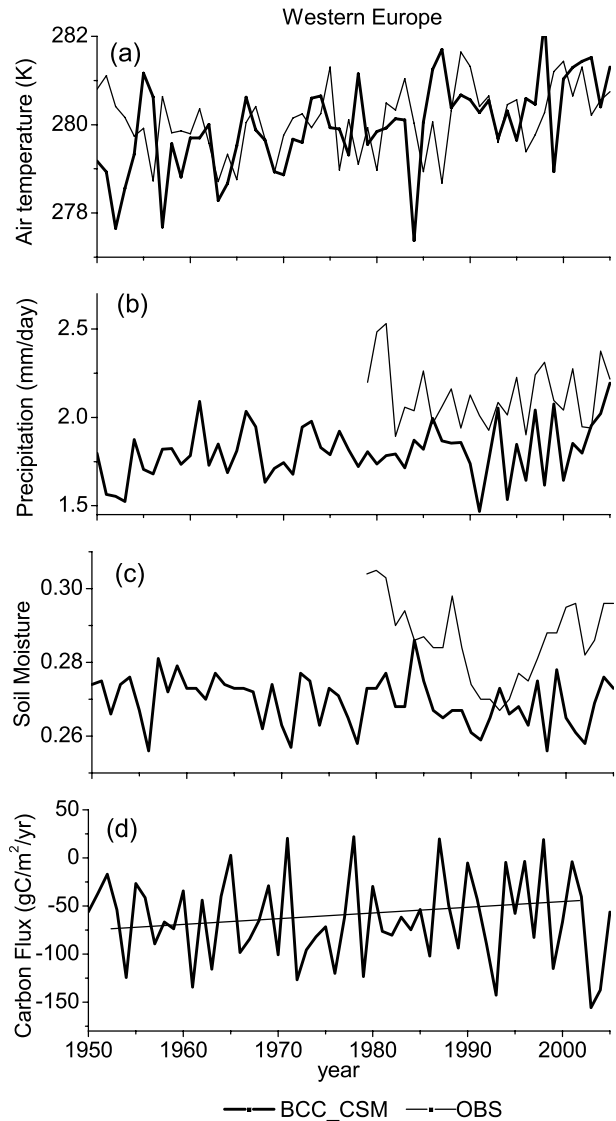


Figure 19. The same as in Figure 16 but for western Europe (15°E – 40°E , 45°N – 60°N).

4. Summary and Discussion

[58] The paper presented the basic performance of the Beijing Climate Center Climate System Model (BCC_CSM1.1) in reproducing the global carbon cycle from 1850 to 2005. BCC_CSM1.1 is a global ocean-atmosphere-land-ice fully coupled model with an interactive carbon cycle. A 300 year preindustrial control experiment and the historical experiment from 1850 to 2005 were conducted by BCC_CSM1.1 with prescribed anthropogenic CO_2 emission and other historical forcing following the CMIP5 recommendation.

[59] BCC_CSM1.1 can well reproduce the global trend and evolution of the atmospheric CO_2 concentration and surface air temperature from 1850 to 2005. There is only 5 ppmv higher than the observation of CO_2 concentration at year 2005. Both land and ocean act as an important carbon sink in the 20th century. Total CO_2 uptakes by the global land and ocean are 3.6 GtC yr^{-1} for the decades of 1980s and 4.0 GtC yr^{-1} for the decades of 1990s. They compared reasonably well to previous observation-based or model estimates.

[60] Regional variation of CO₂ uptake in land is examined in detail. The largest terrestrial CO₂ sink over the globe in BCC_CSM1.1 is distributed in the northern midlatitudes, with three significant carbon sink areas in eastern U.S., eastern China, and western Europe. The Amazon is simulated as a net carbon source to the atmosphere by BCC_CSM1.1. This is related to the fact that the Amazon is an old-aged tropical forest with large carbon storage. It seems that BCC_CSM1.1 underestimates the NPP in the Amazon, due to model biases of insufficient precipitation in this region.

[61] The carbon exchange with the atmosphere in the Amazon is still of large uncertainty. *Rice et al.* [2004] used the observation for a well-drained mature upland forest in the Tapajos National Forest near Santarem, Para, Brazil (2°51'S, 54°58'W) and pointed out that transfer of carbon between live and dead biomass pools can lead to substantial increases in the pool of coarse woody debris and finally cause net carbon release to the atmosphere in this region. Based on a numerical simulation using satellite observations of vegetation cover, *Potter et al.* [2005] predicted a CO₂ source of 0.17 GtC per year in 1983 in the Amazon. In a recent study of *Phillips et al.* [2009], it is shown that if droughts become more frequent in some tropical regions such as in the Amazon in 2005, then the biomass sink may flip into a source. These results indicate that the Amazon may be an area of carbon source under some conditions.

[62] In the last half of the 20th century, there is an obvious increase of carbon uptake by the global land, mainly in the Amazon, eastern North America, and eastern China. However, this increasing trend of the continental carbon uptake in the 20th century cannot be used alone to draw conclusions on climate-carbon feedback that is thought to be positive in most numerical models [*Friedlingstein et al.*, 2006], since the CO₂ concentration has also largely increased during the 20th century. A precise evaluation of the climate-carbon feedback is therefore needed to analyze further appropriately designed sensitivity experiments.

[63] At interannual timescale, BCC_CSM1.1 shows a positive correlation between the net carbon flux (accounted positive from land to atmosphere) and the surface air temperature for most continental areas of low and midlatitudes. We might deduce the positive climate-carbon feedback (warmer temperature leads to smaller land carbon uptake). But we also find a negative correlation between the land carbon uptake and soil moisture, that is, a wetter soil is more favorable for a larger NPP than for a stronger soil respiration, hence a more intense terrestrial carbon uptake. We need to emphasize that such relationships are valid at interannual timescales, but maybe not for a global warming trend. The relative contribution of soil moisture to terrestrial carbon cycle over tropical regions is more important than that of air temperature, but the air temperature is more important than soil moisture over other regions of the globe.

[64] The main spatial pattern of the air-sea CO₂ exchange fluxes is featured as an outgassing of CO₂ to the atmosphere in the equatorial oceans, and an oceanic uptake at higher latitudes, such as the North Pacific and North Atlantic. In comparison to the natural carbon exchange in preindustrial conditions, the anthropogenic carbon uptakes by the global oceans are mainly distributed in the Southern Ocean and North Atlantic.

[65] The interannual variability of atmospheric CO₂ shows remarkable correlation with ENSO. The positive correlation

between the natural variation of global atmospheric CO₂ and the Niño-3 index based on the observation data was reproduced in BCC-CSM1.1. This is mainly attributed to the CO₂ variation in the tropics. Further studies are necessary to investigate ENSO and its impacts on the atmospheric circulation and precipitation, and consequently on the land and ocean carbon uptakes.

[66] Although several recent studies suggested that some potential physical and biogeochemical drivers of the ocean carbon cycle are favorable for a decrease of CO₂ uptake in the Southern Ocean in a warmer climate [e.g., *Sarmiento et al.*, 1998; *Cox et al.*, 2000; *Plattner et al.*, 2002; *Russell et al.*, 2006; *Le Quere et al.*, 2007], the opposite is also found by others [e.g., *Zickfeld et al.*, 2007; *McNeil et al.*, 2001; *Crueger et al.*, 2008; *Matear and Lenton*, 2008], which supports our findings of an increase of oceanic carbon uptake because of the anthropogenic CO₂ emission during the 20th century. For example, *McNeil et al.* [2001] showed an increase in observed CO₂ uptake for the sub-Antarctic oceanic zone between 45°S and 50°S during a time interval of 28 years. Their estimation of the CO₂ uptake ranged from 0.73 to 0.86 μmol kg yr⁻¹ between 1968 and 1996.

[67] The carbon flux in the Southern Ocean is a complex issue. *Matear and Lenton* [2008], by using an ocean biogeochemical model, concluded that the CO₂ uptake in the Southern Ocean remains almost unchanged when climate changes, since two opposite effects almost cancel out each other: an increase in heat and freshwater fluxes can lead to a net increase in the Southern Ocean uptake (south of 40°S), while an increase in wind stresses lead to a net decrease in uptake. As pointed out by *Ito et al.* [2010], the mechanism and pathways of anthropogenic CO₂ uptake and transport are poorly understood. Causes of the increase of CO₂ uptake in the Southern Ocean in BCC_CSM1.1 deserve further investigation.

[68] In this work, anthropogenic land cover change (LCC) is not explicitly included in the land model of BCC_CSM1.1. But the prescribed total anthropogenic CO₂ emission, following the CMIP5 recommendation, does take into account the LCC in the historical simulation. As a result, the radiative effect of CO₂ emission from LCC on the climate is, at least in part, implicitly taken into account in our simulation, albeit the following two processes are missing in the model: (a) the decrease in the sink capacity of the global terrestrial biosphere due to reduction of the residence time of carbon when, for example, forests or grasslands are converted to cultivated land [e.g., *Gitz and Ciais*, 2004]; and (b) the effect of anthropogenic land cover change on climate through changes in the physical properties of the land surface [e.g., *Brovkin et al.*, 2004, 2006; *Betts et al.*, 2007]. The latter process, also neglected in many previously published climate-carbon cycle models, is now included in some (not all) CMIP5 models and will surely be among our objectives in future model development.

[69] We also noticed relatively high carbon sink/source in regional scales after 300 year control run. It is possibly caused by relatively short simulation period to reach the model equilibrium, or existence of the multidecadal to centennial scale drifts at regions in BCC_CSM1.1. More experiments are needed to understand the centennial scale drift in fully coupled climate models in the future.

[70] **Acknowledgments.** This work was supported by National Basic Research Program of China (973 Program:2010CB951902) and Special Program for China Meteorology Trade (Grant No. GYHY201306020).

References

- Arora, V. K., G. J. Boer, J. R. Christian, C. L. Curry, K. L. Denman, K. Zahariev, G. M. Flato, J. F. Scinocca, W. J. Merryfield, and W. G. Lee (2009), The effect of terrestrial photosynthesis down regulation on the twentieth-century carbon budget simulated with the CCCma earth system model, *J. Climate*, *22*, 6066–6088.
- Bacastow, R. (1976), Modulation of atmospheric carbon dioxide by the Southern Oscillation, *Nature*, *261*, 116–118.
- Bacastow, R., E. Maier-Reimer (1990), Ocean-circulation model of the carbon cycle, *Clim. Dyn.*, *4*, 95–125.
- Batjes, N. H. (1996), Total carbon and nitrogen in the soils of the world, *Eur. J. Soil Sci.*, *47* (2), 151–163.
- Betts, R. A., P. D. Falloon, K. K. Goldewijk, and N. Ramankutty (2007), Biogeophysical effects of land use on climate: Model simulations of radiative forcings and large-scale temperature change, *Agric. For. Meteorol.*, *142*, 216–233, doi:10.1016/j.agrformet.2006.08.021.
- Boer, G. J., and V. Arora (2010), Geographic aspects of temperature and concentration feedbacks in the carbon budget, *J. Climate*, *23*, 775–784.
- Bolin, B., and R. Sukumar (2000), Global perspective. in: Land Use, Land-Use Change, and Forestry. Special Report of the IPCC, edited by R. T. Watson, I. R. Noble, B. Bolin, N. H. Ravindranath, D. J. Verardo, D. J. Dokken, Cambridge University Press, Cambridge, UK, 23–51.
- Bonan, G. B., S. Levis, L. Kergoat, K. W. Oleson (2002), Landscapes as patches of plant functional types: An integrating concept for climate and ecosystem model, *Global Biogeochem. Cycles*, *16*(2), 1021, doi:10.1029/2000GB001360.
- Brohan, P., J. J. Kennedy, I. Harris, S. F. B. Tett, and P. D. Jones (2006), Uncertainty estimates in regional and global observed temperature changes: A new dataset from 1850, *J. Geophys. Res.*, *111*, D12106, doi:10.1029/2005JD006548.
- Borken, W., E. A. Davidson, K. Savage, J. Gaudinski, and S. E. Trumbore (2003), Drying and wetting effects on carbon dioxide release from organic horizons, *Soil Sci. Soc. Am. J.*, *67*, 1888–1896.
- Brovkin, V., S. Sitch, W. von Bloh, M. Claussen, E. Bauer, W. Cramer (2004), Role of land cover changes for atmospheric CO₂ increase and climate change during the last 150 years, *Global Change Biol.*, *10*, 1253–1266.
- Brovkin, V., M. Claussen, E. Driesschaert, T. Fichetef, D. Kicklighter, M. F. Loutre, H. D. Matthews, N. Ramankutty, M. Schaeffer, S. Sokolov (2006), Biogeophysical effects of historical land cover changes simulated by six Earth system models of intermediate complexity, *Clim. Dyn.*, *26*, 587–600, doi:10.1007/s00382-005-0092-6.
- Cadule, P., P. Friedlingstein, L. Bopp, S. Sitch, C. D. Jones, P. Ciais, S. L. Piao, and P. Peylin (2010), Benchmarking coupled climate-carbon models against long-term atmospheric CO₂ measurements, *Global Biogeochem. Cycles*, *24*, GB2016, doi:10.1029/2009GB003556.
- Cao, M., and F. I. Woodward (1998), Net primary and ecosystem production and carbon stocks of terrestrial ecosystems and their responses to climate change, *Global Change Biol.*, *4*, 185–198.
- Churkina, G., et al. (2010), Interactions between nitrogen deposition, land cover conversion, and climate change determine the contemporary carbon balance of Europe, *Biogeosci. Discuss.*, *7*, 2227–2265.
- Collins, W. D., and Coauthors (2004), Description of the NCAR community atmosphere model (CAM3). Technical Report NCAR/TN-464+STR, National Center for Atmospheric Research, Boulder, Colorado, 226 pp.
- Cox, P. M., R. A. Betts, C. D. Jones, S. A. Spall, and I. J. Totterdell (2000), Acceleration of global warming due to carbon cycle feedbacks in a coupled climate model, *Nature*, *408*, 184–187.
- Cox, P. M., R. A. Betts, M. Collins, P. P. Harris, C. Huntingford, and C. D. Jones (2004), Amazonian forest dieback under climate-carbon cycle projections for the 21st century, *Theor. Appl. Climatol.*, *78*, 137–156.
- Cramer, W., and Coauthors (2001), Global response of terrestrial ecosystem structure and function to CO₂ and climate change: Results from six global dynamic vegetation models, *Global Change Biol.*, *7*, 357–373.
- Cramer, W., D. W. Kicklighter, A. Bondeau, B. Moore, G. Churkina, B. Nemry, A. Ruimy, A. L. Schloss, and the participants of the Potsdam NPP Model Intercomparison (1999), Comparing global models of terrestrial net primary productivity (NPP): Overview and key results, *Global Change Biol.*, *5*, (suppl. 1), 1–15.
- Crueger, T., E. Roeckner, T. Raddatz, R. Schnur, P. Wetzzel (2008), Ocean dynamics determine the response of oceanic CO₂ uptake to climate change, *Clim. Dyn.*, *31*, 151–168, doi:10.1007/s00382-007-0342-x.
- Denman, K.L., et al. (2007), Couplings between changes in the climate system and biogeochemistry. *Climate Change 2007: The Physical Science Basis*, edited by S. Solomon, et al., 589–662, Cambridge University Press, Cambridge, United Kingdom and New York, N.Y., USA.
- Doney, S. C., K. Lindsay, I. Fung, and J. John (2006), Natural variability in a stable, 1000-yr global coupled climate-carbon cycle simulation, *J. Climate*, *19*, 3033–3054.
- Dufresne, J.-L., P. Friedlingstein, M. Berthelot, L. Bopp, P. Ciais, L. Fairhead, H. Le Treut, P. Monfray (2002), On the magnitude of positive feedback between future climate change and the carbon cycle, *Geophys. Res. Lett.*, *29*, 1405, doi:10.1029/2001GL013777.
- Eby, M., K. Zickfeld, A. Montenegro, D. Archer, K. J. Meissner, and A. J. Weaver (2009), Lifetime of anthropogenic climate change: Millennial time scales of potential CO₂ and surface temperature perturbations, *J. Climate*, *22*, 2501–2511.
- Friedlingstein, P., L. Bopp, P. Ciais, J.-L. Dufresne, L. Fairhead, H. LeTreut, P. Monfray, and J. Orr (2001), Positive feedback between future climate change and the carbon cycle, *Geophys. Res. Lett.*, *28*, 1543–1546.
- Friedlingstein, P., J.-L. Dufresne, P. Cox, P. Rayner (2003), How positive is the feedback between climate change and the carbon cycle, *Tellus*, *55B*, 692–700.
- Friedlingstein, P., et al. (2006), Climate-carbon cycle feedback analysis: Results from the C4MIP model intercomparison, *J. Climate*, *19*, 3337–3353.
- Friedlingstein, P., and I. C. Prentice (2010), Carbon-climate feedbacks: A review of model and observation based estimates, *Curr. Opin. Environ. Sustain.*, *2*, 251–257.
- Gitz, V., and P. Ciais (2004), Future expansion of agriculture and pasture acts to amplify atmospheric CO₂ levels in response to fossil-fuel and land-use change emissions, *Clim. Chang.*, *67*, 161–184.
- Gregory, J. M., C. D. Jones, P. Cadule, P. Friedlingstein (2009), Quantifying carbon cycle feedbacks, *J. Clim.*, *22*, 5232–5250.
- Griffies, S. M., et al. (2005), Formulation of an ocean model for global climate simulations, *Ocean Sci.*, *1*, 45–79.
- Gurney, K. R., et al. (2002), Towards robust regional estimates of CO₂ sources and sinks using atmospheric transport models, *Nature*, *415*, 626–630.
- Houghton, J. T., Y. Ding, D. J. Griggs, M. Noguer, P. J. van der Linden, and D. Xiaosu (2001), *Climate Change 2001: The Scientific Basis*, 881 pp, Cambridge University Press, Cambridge, United Kingdom and New York, N.Y., USA.
- Houghton, R. A. (2003), Why are estimates of the terrestrial carbon cycle balance so different?, *Glob. Chang. Biol.*, *9*, 500–509.
- House, J. I., I. C. Prentice, N. Ramankutty, R. A. Houghton, and M. Heimann (2003), Reconciling apparent inconsistencies in estimates of terrestrial CO₂ sources and sinks, *Tellus*, *55B*, 345–363.
- Hunke, E. C., and J. K. Dukowicz (1997), An elastic-viscous-plastic model for sea ice dynamics, *J. Phys. Oceanogr.*, *27*, 1849–1867.
- Ito, T., M. Woloszyn, and M. Mazloff (2010), Anthropogenic carbon dioxide transport in the Southern Ocean driven by Ekman flow, *Nature*, *463*, 80–84.
- Janssens, I. A., et al. (2003), Europe's terrestrial biosphere absorbs 7 to 12% of European anthropogenic CO₂ emissions, *Science*, *300*, 1538–1542.
- Ji, J. (1995), A climate-vegetation interaction model: Simulating physical and biological processes at the surface, *J. Biogeogr.*, *22*, 2063–2069.
- Ji, J., M. Huang, and K. Li (2008), Prediction of carbon exchange between China terrestrial ecosystem and atmosphere in 21st century, *Sci. China Ser.D: Earth Sci.*, *51*(6), 885–898.
- Jones, C. D., M. Collins, P. M. Cox, S. A. Spall (2001), The carbon cycle response to ENSO: A coupled climate-carbon cycle model study, *J. Climate*, *14*, 4113–4129.
- Kimble, J. M., H. Eswaran, T. Cook (1990), Organic carbon on a volume basis in tropical and temperate soils, *Transactions of the 14th Int. Congr. Soil Sci.*, *5*, 248–253.
- Koffi, E. N., P. J. Rayner, M. Scholze, and C. Beer (2012), Atmospheric constraints on gross primary productivity and net ecosystem productivity: Results from a carbon-cycle data assimilation system, *Global Biogeochem. Cycles*, *26*, GB1024, doi:10.1029/2010GB003900.
- Le Quére, C. (2010), Trends in the land and ocean carbon uptake, *Curr. Opin. Environ. Sustain.*, *2* (4), 219–224. 10.1016/j.cosust.2010.06.003.
- Le Quere, C., et al. (2007), Saturation of the Southern Ocean CO₂ sink due to recent climate change, *Science*, *316*, 1735–1738, doi:10.1126/science.1136188.
- Le Treut, H., R. Somerville, U. Cubasch, Y. Ding, C. Mauritzen, A. Moksit, T. Peterson, M. Prather (2007), Historical Overview of Climate Change. in: *Climate Change 2007: The Scientific Basis. Contribution of Working Group I to the Fourth Assessment Report of the Intergovernmental Panel on Climate Change*, edited by S. Solomon, D. Qin, M. Manning, Z. Chen, M. Marquis, K. B. Averyt, M. Tignor, H. L. Miller, pp 93–127, Cambridge University Press, Cambridge.

- Liu, Z., W. Dreybrodt, and H. Wang (2010), A new direction in effective accounting for the atmospheric CO₂ budget: Considering the combined action of carbonate dissolution, the global water cycle and photosynthetic uptake of DIC by aquatic organisms, *Earth Sci. Rev.*, *99*, 162–172.
- Lu, J. H., and J. J. Ji (2006), A simulation and mechanism analysis of long-term variations at land surface over arid/semi-arid area in north China, *J. Geophys. Res.*, *111*, D09306, doi:10.1029/2005JD006252.
- Ludwig, W., P. Amiotte-Suchet, J. L. Probst (2011), ISLSCP II global river fluxes of carbon and sediments to the oceans. in: ISLSCP Initiative II Collection, edited by F.G. Hall, G. Collatz, B. Meeson, S. Los, E. Brown de Colstoun, and D. Landis, Oak Ridge National Laboratory Distributed Active Archive Center, Oak Ridge. Data set is available on-line [http://daac.ornl.gov/].
- Malhi, Y., A. D. Nobre, J. Grace, B. Kruijt, M. G. P. Pereira, A. Culf, and S. Scott (1998), Carbon dioxide transfer over a Central Amazonian rain forest, *J. Geophys. Res.*, *103*(D24), 31,593–31,612, doi:10.1029/98JD02647.
- Malhi, Y. (2010), The carbon balance of tropical forest regions, 1990–2005, *Curr. Opin. Environ. Sustain.* *2010*, (2), 237–244.
- Matear, R. J., A. Lenton (2008), Impact of historical climate change on the southern ocean carbon cycle, *J. Climate*, *21*, 5820–5834.
- Matthews, H. D., A. J. Weaver, and K. J. Meissner (2005), Terrestrial carbon cycle dynamics under recent and future climate change, *J. Climate*, *18*, 1609–1628.
- McNeil, B. I., R. J. Matear, R. M. Key, J. L. Bullister, and J. L. Sarmiento (2003), Anthropogenic CO₂ uptake by the ocean based on the global chlorofluorocarbon data set, *Science*, *299*, 235–239.
- McNeil, B. I., B. Tilbrook, and R. J. Matear (2001), Accumulation and uptake of anthropogenic CO₂ in the Southern Ocean, south of Australia between 1968 and 1996, *J. Geophys. Res.*, *106*(C12), 31,431–31,445.
- Meehl, G. A., and Coauthors (2007), Global climate projections. Climate Change 2007: The physical science basis, edited by S. Solomon, et al. 747–845, Cambridge University Press, Cambridge, United Kingdom and New York, N.Y., USA.
- Meinshausen, M., et al. (2011), The RCP greenhouse gas concentrations and their extension from 1765 to 2300, *Clim. Chang.*, *109*, 213–241, doi:10.1007/s10584-011-0156-z.
- Murakami, K., T. Sasai, Y. Yamaguchi (2010), A new one-dimensional simple energy balance and carbon cycle coupled model for global warming simulation, *Theor. Appl. Climatol.*, *101*, 459–473, doi:10.1007/s00704-009-0232-8.
- Murray, R. J. (1996), Explicit generation of orthogonal grids for ocean models, *J. Comput. Phys.*, *126*, 251–273.
- Nemani, R. R., C. D. Keeling, H. Hashimoto, W. M. Jolly, S. C. Piper, C. J. Tucker, R. B. Myneni, and S. W. Running (2003), Climate-driven increases in global terrestrial net primary production from 1982 to 1999, *Science*, *300*, 1560–1563.
- Nemani, R., et al. (2002), Recent trends in hydrologic balance have enhanced the terrestrial carbon sink in the United States, *Geophys. Res. Lett.*, *29*(10), 1468, doi:10.1029/2002GL014867.
- Nunes, E. L., M. H. Costa, A. C. M. Malhado, L. C. P. Dias, S. A. Vieira, L. B. Pinto, R. J. Ladle (2012), Monitoring carbon assimilation in South America's tropical forests: Model specification and application to the Amazonian droughts of 2005 and 2010, *Remote Sens. Environ.*, *117*, 449–463.
- Oleson, K.W., Y. Dai, et al. (2004), Technical description of the Community Land Model (CLM). NCAR Tech. Note TN-461+STR, 174 pp.
- Pan, Y., R. A. Birdsey, J. Fang, et al. (2011), A large and persistent carbon sink in the world's forests, *Science*, *333*, 988–993.
- Parton, W. J., W. B. Stewart, and C. V. Cole (1988), Dynamics of C, N, P and S in grassland soils: A model, *Biogeochemistry*, *5*, 109–131.
- Piao, S., P. Ciais, P. Friedlingstein, N. de Noblet-Ducoudre, P. Cadule, N. Viovy, T. Wang (2009a), Spatiotemporal patterns of terrestrial carbon cycle during the 20th century, *Global Biogeochem. Cycles*, *23*, GB4026, doi:10.1029/2008GB003339.
- Piao, S., J. Fang, P. Ciais, P. Peylin, Y. Huang, S. Sitch, T. Wang (2009b), The carbon balance of terrestrial ecosystem in China, *Nature*, *458*, 1009–1013.
- Phillips, O. L., et al. (2009), Drought sensitivity of the Amazon rainforest, *Science*, *323*, 1344–1347.
- Platner, G.-K., F. Joos, and T. F. Stocker (2002), Revision of the global carbon budget due to changing air-sea oxygen fluxes, *Global Biogeochem. Cycles*, *16*(4), 1096, doi:10.1029/2001GB001746.
- Potter, C. S., S. A. Klooster, P. Tan, M. Steinbach, V. Kumar, V. Genovese (2005), Variability in terrestrial carbon sinks over two decades. Part III: South America, Africa, and Asia, *Earth Interac.*, *9* (No. 29), 1–14.
- Potter, C. S., S. A. Klooster, R. B. Myneni, V. Genovese, P.-N. Tan, and V. Kumar (2003), Continental scale comparisons of terrestrial carbon sinks estimated from satellite data and ecosystem modeling 1982–1998, *Global Planet. Change* *39*, 201–213.
- Prentice, I. C., et al. (2001), The carbon cycle and atmospheric CO₂. in: The Intergovernmental Panel on Climate Change (IPCC) Third Assessment Report, edited by J. T. Houghton, Y. Ding, pp 185–237, Cambridge University Press, New York, chap. 3.
- Prentice, I. C., and J. Lloyd (1998), C-quest in the Amazon Basin, *Nature*, *396*, 619–620.
- Raddatz, T. J., C. H. Reick, W. Knorr, J. Kattge, E. Roeckner, R. Schnur, K.-G. Schnitzler, P. Wetzel, J. Jungclaus (2007), Will the tropical land biosphere dominate the climate-carbon cycle feedback during the twenty-first century?, *Clim. Dyn.*, *29*, 565–574.
- Randerson, J., et al. (2009), Systematic assessment of terrestrial biogeochemistry in coupled climate-carbon models, *Glob. Chang. Biol.*, *15*, 2462–2484, doi:10.1111/j.1365-2486.2009.01912.x.
- Rice, A. H., E. H. Pyle, S. R. Saleska, L. Hutyrá, M. Palace, M. Keller, P. B. D. Camargo, K. Portilho, D. F. Maroues, and S. C. Wofsy (2004), Carbon balance and vegetation dynamics in an old-growth Amazonian forest, *Ecol. Appl.*, *14*(4) Supplement: S55–S71.
- Roedenbeck, C., S. Houweling, M. Gloor, and M. Heimann (2003), CO₂ flux history 1982–2001 inferred from atmospheric data using a global inversion of atmospheric transport, *Atmos. Chem. Phys.*, *3*, 1919–1964.
- Roesch, A., M. Wild, H. Gilgen, and A. Ohmura (2001), A new snow cover fraction parameterization for the ECHAM4 GCM, *Clim. Dyn.*, *17*, 933–946.
- Roy, T., L. Bopp, M. Gehlen, B. Schneider, P. Cadule, T. L. Frolicher, J. Segschneider, J. Tjipultra, C. Heinze, F. Joos (2011), Regional impacts of climate change and atmospheric CO₂ on future ocean carbon uptake: A multimodel linear feedback analysis, *J. Climate*, *24*, 2300–2318.
- Running, S. W., R. R. Nemani, F. A. Heinsch, M. Zhao, M. Reeves, and H. Hashimoto (2004), A continuous satellite-derived measure of global terrestrial primary production, *Bioscience*, *54*, 547–560.
- Russell, J. L., K. W. Dixon, A. Gnanadesikan, R. J. Stouffer, and J. R. Toggweiler (2006), The Southern Hemisphere westerlies in a warming world: Propping open the door to the deep ocean, *J. Climate*, *19*, 6382–6390.
- Sarmiento, J. L., T. M. C. Hughes, and R. J. Stouffer (1998), Simulated response of the ocean carbon cycle to anthropogenic climate warming, *Nature*, *393*, 245–249.
- Sarmiento, J. L., and C. Le Quéré (1996), Oceanic carbon dioxide in a model of century-scale global warming, *Science*, *274*, 1346–1350.
- Sarmiento, J. L., and E. T. Sundquist (1992), Revised budget for the oceanic uptake of anthropogenic carbon dioxide, *Nature*, *356*, 589–593.
- Savage, K. E., and E. A. Davidson (2001), Interannual variation of soil respiration in two New England forests, *Global Biogeochem. Cycles*, *15*(2), 337–350.
- Schulze, E. D., S., et al. (2009), Importance of methane and nitrous oxide for Europe's terrestrial greenhouse-gas balance, *Nat. Geosci.*, *2*, 842–850.
- Senna, M. C. A., M. H. Costa, L. I. C. Pinto, H. M. A. Imbuzeiro, L. M. F. Diniz, and G. F. Pires (2009), Challenges to reproduce vegetation structure and dynamics in Amazonia using a coupled climate-biosphere model, *Earth Interac.*, *13* (11), 1–28.
- Sombroek, W. G., F. O. Nachtergaele, A. Hebel (1993), Amounts, dynamics and sequestrations of carbon in tropical and subtropical soils, *Ambio*, *22*, 417–426.
- Stephens, B. B., et al. (2007), Weak northern and strong tropical land carbon uptake from vertical profiles of atmospheric CO₂, *Science*, *316* (5832), 1732–1735, doi:10.1126/science.1137004.
- Takahashi, T., et al. (2009), Climatological mean and decadal change in surface ocean pCO₂, and net sea-air CO₂ flux over the global oceans, *Deep Sea Res. II*, *56*, 554–577.
- Tans, P. P., I. Fung, T. Takahashi (1990), Observational constraints on the global atmospheric CO₂ budget, *Science*, *247*, 1331–1439.
- Taylor, K. E., R. J. Stouffer, and G. A. Meehl (2009), A Summary of the CMIP5 experiment design, <http://www.pcmdi.llnl.gov/>.
- Torrence and Compo (1998), A practical guide to wavelet analysis, *Bull. Am. Meteorol. Soc.*, *79*, 61–78.
- Trenberth, K. E., et al. (2007), Observations: surface and atmospheric climate change. in Climate Change 2007: The Physical Science Basis, edited by S. Solomon, D. Qin, M. Manning, Z. Chen, M. Marquis, K. B. Averyt, M. Tignor, and H. L. Miller, pp. 235–336. Cambridge University Press, Cambridge, United Kingdom and New York, N.Y., USA.
- Vichi, M., E. Manzini, P. G. Fogli, A. Alessandri, L. Patara, E. Scoccimarro, S. Masina, A. Zavarra (2011), Global and regional ocean carbon uptake and climate change: Sensitivity to a substantial mitigation scenario, *Clim. Dyn.*, *37*, 1929–1947, doi:10.1007/s00382-011-1079-0.
- Wanninkhof, R. (1992), Relationship between wind-speed and gas exchange over the ocean, *J. Geophys. Res.*, *97*, 7373–7382.
- Welp, L. R., R. K. Keeling, H. A. J. Meijer, A. F. Bollenbacher, S. C. Piper, K. Yoshimura, R. J. Francey, C. E. Allison, and M. Wahlen (2011), Interannual variability in the oxygen isotopes of atmospheric CO₂ driven by El Niño, *Nature*, *477*, 579–582.

- Wigley, T. M. L. (2005), The climate change commitment, *Science*, *307*, 1766–1769.
- Winton, M. (2000), A reformulated three-layer sea ice model, *J. Atmos. Oceanic Technol.*, *17*, 525–531.
- Wu, T. (2012), A mass-flux cumulus parameterization scheme for large-scale models: Description and test with observations, *Clim. Dyn.*, *38*, 725–744, doi:10.1007/s00382-011-0995-3.
- Wu, T., R. Yu, and F. Zhang (2008), A modified dynamic framework for atmospheric spectral model and its application, *J. Atmos. Sci.*, *65*, 2235–2253.
- Wu, T., R. Yu, F. Zhang, Z. Wang, M. Dong, L. Wang, X. Jin, D. Chen, L. Li (2010), The Beijing climate center for atmospheric general circulation model (BCC-AGCM2.0.1): Description and its performance for the present-day climate, *Clim. Dyn.*, *34*, 123–147.
- Xiao, J., Q. Zhuang, E. Liang, D. McGuire, A. Moody, D. W. Kicklighter, X. Shao, and J. M. Melillo (2009), Twentieth-century droughts and their impacts on terrestrial carbon cycling in China, *Earth Interact.*, *13* (10), 1–31.
- Yamanaka, Y., and E. Tajika (1996), The role of the vertical fluxes of particulate organic matter and calcite in the oceanic carbon cycle: Studies using an ocean biogeochemical general circulation model, *Global Biogeochem. Cycles*, *10*(2), 361–382, doi:10.1029/96GB00634.
- Yang, Z.-L., R. E. Dickinson, A. Robock, K. Y. Vinnikov (1997), Validation of the snow submodel of the biosphere–atmosphere transfer scheme with Russian snow cover and meteorological observational data, *J. Climate*, *10*, 353–373.
- Zeng, N., H. Qian, E. Munoz, and R. Iacono (2004), How strong is carbon-climate feedback under global warming?, *Geophys. Res. Lett.*, *31*, L20203, doi:10.1029/2004GL020904.
- Zhang, L., H. Zhang, and Y. Li (2009), Surface energy, water and carbon cycle in China simulated by the Australian community land surface model (CABLE), *Theor. Appl. Climatol.*, *96*, 375–394, doi:10.1007/s00704-008-0047-z.
- Zhao, M., S. W. Running, and R. R. Nemani (2006), Sensitivity of Moderate Resolution Imaging Spectroradiometer (MODIS) terrestrial primary production to the accuracy of meteorological reanalysis, *J. Geophys. Res.*, *111*, G01002, doi:10.1029/2004JG000004.
- Zickfeld, K., J. C. Fyfe, O. A. Saenko, M. Eby, and A. J. Weaver (2007), Response of the global carbon cycle to human-induced changes in Southern Hemisphere winds, *Geophys. Res. Lett.*, *34*, L12712, doi:10.1029/2006GL028797.
- Zickfeld, K., M. Eby, H. D. Matthews, A. Schmittner, A. J. Weaver (2011), Nonlinearity of carbon cycle feedbacks, *J. Climate*, *24*, 4255–4275, doi:10.1175/2011JCLI3898.1.